Hochschule Karlsruhe
Technik und Wirtschaft
UNIVERSITY OF APPLIED SCIENCES

MASTER THESIS

BOARD DESIGN FOR A CITIZEN-SCIENCE COSMIC RAY MUON DETECTOR

by

Swathy Ramakrishnan
Matrikel Number - 66125

Supervisor: **Prof. Dr. Michael Schmelling**
Referee: **Prof. Dr. Michael Bantel**
Co-Referee: **Prof. Dr. techn. Herman-Jalli Ng**
Master Thesis Number: **529**
Duration: ***15 January 2020 till 15 August 2020***

15 August, 2020

ABSTRACT

The main aim of this project is to develop a printed circuit board for a cosmic ray muon detector with primary use for citizen science. Compared to the previous versions of the detector, the goals were to reduce the low frequency noise levels in the output and to improve the general board layout and functionality. The study of cosmic rays aids to reduce the electronic errors in consumer electronics and satellites along with quantifying the health impact of this natural radiation. Cosmic rays which contain mainly protons and nuclei interact in the upper atmosphere and produce muons that can reach the earth's surface. These are then detected using photo diodes. The resulting signal is amplified using a charge sensitive preamplifier followed by a high-pass filter thereby allowing to reduce the unwanted noise and helping to obtain a strong signal.

DECLARATION

I declare that this Master Thesis entitled "Board Design for a Citizen Cosmic Ray Muon Detector" is my original work. The project was done in the premises of Max Planck Institute for nuclear physics under the guidance and supervision of Prof. Dr Michael Schmelling, Max Planck Institute für Kernphysik and Prof. Dr. rer. nat. Michael Bantel, Hochschule Karlsruhe Technik und Wirtschaft.

I declare that all observations and results are solely mine and have not been published by or in any other sources. Any references used for the work have been cited at the respective position and listed in the References.

This Master Thesis is submitted as a part of M.Sc. Sensor System Technology at Hochschule Karlsruhe – Technik und Wirtschaft.

I declare that this Thesis has been solely written by me and no other references, other than the ones cited here in the report has been used during the preparation.

15/08/2020, Ramakrishnan, Swathy

Date, Signature (Last name, first name)

ACKNOWLEDGEMENT

With great gratitude, I would like to acknowledge all those who helped me to complete my project.

I express my heartfelt thanks to Prof. Dr. James Anthony Hinton, Max Planck Institute für Kernphysik, for giving me an opportunity to work on this project.

I express my sincere thanks to Prof. Dr. rer. nat. Michael Bantel, supervisor, and Prof. Dr. techn. Herman-Jalli Ng, Secondary Supervisor, Hochschule Karlsruhe for the suggestions and the keen interest shown towards my project.

I express my deep gratitude to Prof. Dr. Michael Schmelling, Supervisor, the suggestions, constant inspiration, and constructive criticisms for the Thesis.

I would also like to express my gratitude to Mr. Hendrik Borras, Project Head, for his constant support and guidance as well as Ms. Priyanka Kesavadas, Colleague, for her contributions to the successful completion of this project.

I sincerely thank all the members of electronics department for their help in the development of the project, especially, Mr. Christian Föhr, for his valuable suggestions and help extended towards the successful completion of this Thesis. Words are few but feelings are more to appreciate my family and friends for the constant support and encouragement provided for my Thesis and also for reviewing this document and for giving me valuable suggestions.

CONTENTS

CHAPTER -1
Introduction

1.1 Overview

This Master Thesis is part of a project that aims at the development of a detector for cosmic ray muons suitable for citizen science. The whole setup uses off-the-shelf electronic components with PIN diodes as the active detector elements to record passing muons. Since the active area of a single PIN diode is only a few square millimetres, many diodes are needed to reach acceptable count rates for the typical muon flux of 1 per square centimetre and minute. The work described here focuses on the design of two PCBs with a low-noise amplifier that is able to read out up to 50 diodes in parallel. To minimise cost, as few active elements as possible are employed. Two boards are needed for a coincidence setup that records passing muons and allows for an efficient rejection of spurious signals from only a single diode. For integration into a PC-based readout system the whole system is designed such that it is able to run using the power supplied by a standard USB port.

1.2 Max-Planck-Institute für Kernphysik

The Max-Planck-Institute für Kernphysik (MPIK), Heidelberg, is a research centre established by the Max Planck Gesellschaft (Max Planck Society) in the year 1958. The MPIK mainly focus on research in the field of Astroparticle Physics and Quantum Dynamics. There are five scientific divisions and many research and junior groups. The five major departments are Stored and Cooled ions, Non-Thermal Astrophysics, Theoretical Quantum Dynamics and Quantum Electrodynamics, Quantum Dynamics and Control and Particle and Astroparticle Physics.

Non-Thermal Astrophysics is the division managed by Prof. Jim Hinton. In this division, research is conducted in two main areas: high-energy astrophysics and particle physics along with conducting experiments such as the GERDA or LEGEND. High energy astrophysics studies the sources and acceleration process of high-energy particles in our universe. For this the group uses atmospheric Cherenkov telescopes or dense particle detector arrays to measure gamma rays emitted by high-energy particles in our Galaxy and beyond.

1.3 Objective

The main aim of this project is to make particle physics more accessible to the general public. This can be achieved by designing a low-cost detector ideally in the range below 100 Euro, which can be easily accessed by schools and citizens. This enables them to get cheaper and easier alternatives to observe cosmic ray muons anywhere. The project mainly focuses on developing two boards to detect cosmic ray muons and to reduce the noise levels in the outputs. It involves the development of an amplifier circuit which can read 50 diodes simultaneously with very little noise. The only constraint in the design being that the incoming signals and the noise should be distinguishable and keeping the cost low by using as few active elements as possible.

1.4 Motivation

Cosmic ray muon detection aids to the reduction in the errors caused in electronic devices and further development of several applications using muon absorption and deflection. The conventional method used for the detection of cosmic ray muons makes use of scintillators and photo multipliers, which often amounts to a price tag above 1000€ [21], and which makes it difficult for most

people to access such equipment. Multiple projects across the world are concerned with developing cost-effective Muon detectors for citizen science, such as CosmicPi [7] and the outreach division of DESY Zeuthen [8]. Development of cosmic ray muon detectors within a given budget is therefore the prime motivation behind the Master Thesis.

A basic circuit to achieve this goal was tested successfully in the version 2 board of the detector, called Silex version 2 board. To reduce cost and increase the availability of parts, off-the-shelf components and few active components were used. PIN diodes as particle detectors were used as a cheaper alternative than the scintillators and photomultipliers. The main issue faced in this board was the low frequency noise that needed to be removed and poor signal output. The work flow of this Master Thesis is as follows. First, we need to design a high-pass filter circuit which can effectively eliminate the low frequency noise in the Silex version 2 board. Secondly, we need to add an Impedance-decoupling to match the impedance of the board to the input impedance of the microcontroller. Thirdly, we need to design a version 3 board incorporating all the changes made in the Silex version 2 board along with various new improvements using KiCAD. And lastly, we must optimize this circuit, with respect to signal strength, while trying to work as much as possible with cost effective components.

CHAPTER 2
THEORY

2.1. Cosmic Ray and Muons

Cosmic rays are high-energy particles which move through space at nearly the speed of light. They mainly consist of protons and alpha particles with a small fraction of heavier nuclei and other subatomic particles such as electrons, positrons and antiprotons. They are known to originate either from the sun or from outside of the solar system and from distant galaxies, which is currently under research. When cosmic rays reach the earth's atmosphere, they interact with the atmosphere and produce showers of secondary particles which results in the generation of electrons, muons and gamma rays [2],[3].

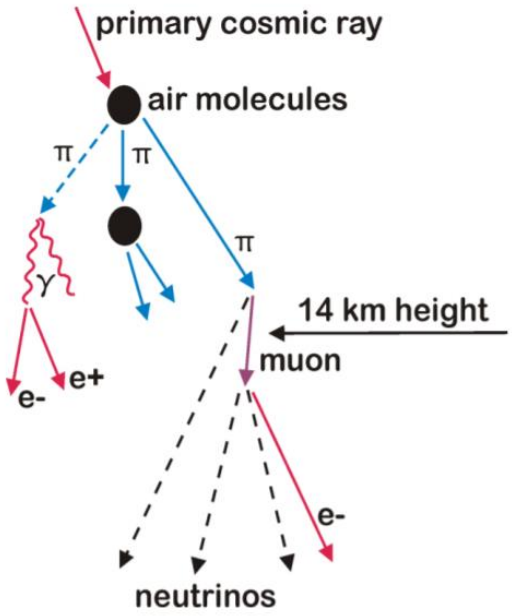

Fig 1. Muon creation and decay [2]

Cosmic ray muons are created when cosmic rays enter earth's atmosphere where they collide with air molecules and this collision initiates a shower (a cascade) of secondary particles, mostly pions. Pions can either be neutral or charged and decay quickly due to their short lifetime. Neutral pions (π^0) decay into two gamma rays, which in turn generate electromagnetic showers (e^+, e^-)

that are not very penetrating. Charged pions (π^+, π^-) will decay in-flight into muons (μ^+, μ^-) and neutrinos [4]. Muons were discovered in cosmic rays by C. Anderson and S.H. Neddermeyer in 1937 [4]. They are essentially heavy versions of the electron, though lighter than protons and neutrons, which makes them unstable. A small fraction of the muons created in cosmic ray showers reach the earth's surface. Some muons further decay into one electron and two neutrinos [3],[4]. Since the muons and electrons of cosmic rays can ionize silicon, they readily cause errors in electronic Instruments. The detection of muons makes it possible to study muon absorption, which in turn can be used to probe the interiors of natural and man- made structures. Looking into the deflection or scattering of muons also leads to a wide range of applications like producing 2-D and 3-D images of the interiors of hidden volumes [5].

CHAPTER 3
Experimental set up

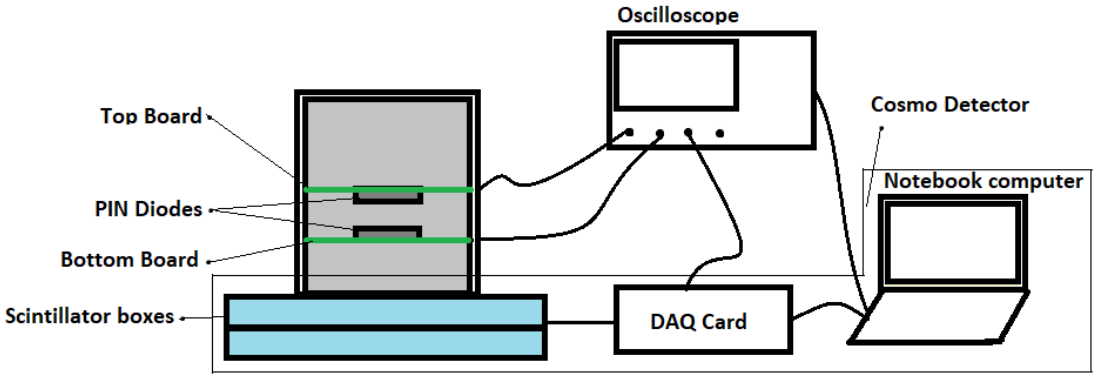

Fig 2. Experimental set up

The experimental set up for the project is as shown in Figure 2. It mainly consists of a CosMO detector, which is explained in more detail in the next section, and the cosmic ray muon detector (Silex version 1 board/ Silex version 2 board/ Silex version 3 board) which consists of a top board, and a bottom board enclosed within a light-tight insulation box. The outputs of the top board, bottom board and the CosMO detector are connected to the oscilloscope in order to view the outputs. Each part of the experimental set up is described below.

3.1 CosMO Detector

A CosMO detector is used in order to study cosmic ray(muons). It is used in this Master Thesis as a reference system to check for coincidences with the test system. The CosMO detector mainly consists of three parts:
Organic scintillators for radiation detection, DAQ (Data Acquisition) card and a notebook computer used to control the DAQ readout and acquire the data for further analysis. We use a set of two scintillator boxes, which consist of an organic scintillator along with a silicon photomultiplier and an amplifier. These

boxes are connected to the DAQ card. The DAQ card can be controlled by the notebook computer to set the coincidence conditions and thresholds.

Scintillators are transparent materials that emit light when ionizing radiation passes through it. When particles or radiation pass through a scintillating material, they excite atoms or molecules in the material, which in turn causes light emission. This is known as scintillation. The light produced is then collected and analysed. In this Master Thesis, two scintillator boxes are used. Each box contains a 20x20 cm^2 organic scintillator slab. The light that is produced when radiation passes is detected by silicon photo-multipliers (SiPMs) and converted into an electric pulse which is then amplified and given to the DAQ card.

The DAQ-card can be used to discriminate pulses and look for coincidences between multiple channels. The DAQ card is then attached to a notebook computer using a USB connection, which enables a direct communication channel between the computer and the DAQ card. This communication channel makes it possible to retrieve the data obtained with the DAQ card [8],[9].

An additional digital output from the Cosmo detector is also given to the oscilloscope in order to check for coincidences with the newly designed cosmic ray muon detector.

3.2 Oscilloscope

The oscilloscope used in this Master Thesis is a Lecroy HDO 6104-MS, which is 1GHz high definition mixed signal oscilloscope. It has four analog input channels, touch screen, USB ports and ethernet ports to export data, 12-bit ADC resolution, advanced math and measurement parameters which can be used to quantify analog and digital waveforms, advanced triggering with trigger scan and measurement trigger which ensures that even complicated signals can be

captured. The signals from the top board, bottom board and Cosmo detector are viewed using the oscilloscope.

3.3 PIN Diode

The PIN diode is the primary active element used in the circuit as the particle detector. A PIN diode is similar to a normal PN-diode except that it has an additional intrinsic layer between the heavily doped p-type and n-type regions. The intrinsic layer is mostly crystal or lightly doped crystal of Silicon or Germanium. When a reverse bias is applied, the PIN- diode acts like a capacitor and can be used as a photodetector [6]. The main advantage of using a PIN diode in the circuitry is that they are more readily available and much cheaper than the conventional detectors like the SiPMs and scintillators. It also generates near instant ionization which makes it a good option for this project.

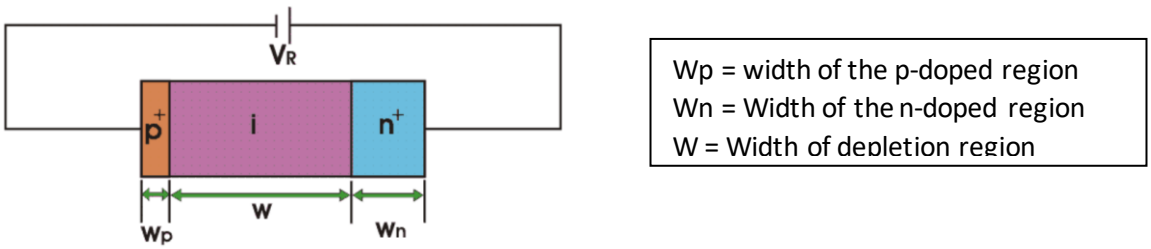

Fig 3. PIN diode in reverse bias [5]

When passing ionising radiation reaches the surface of the PIN-diodes electron-hole generation takes place leading to instant ionisation and thereby generates charges in the diode. These charges can then be absorbed on each side of the diode and the resulting current can be measured. In reverse bias, the width of the depletion region increases due to the presence of the intrinsic layer and therefore more volume for ionisation is available making the detector more efficient. [9]

CHAPTER 4
SILEX DETECTORS

The cosmic ray muon detector designed in this project was named Silex detector. There are three versions of the Silex detector that are tested till date. They are explained in detail in the following section.

4.1 Silex Version 1 Board

The first version of the cosmic ray muon detector (the most recent version being the Silex version 3 board) was developed 2 years back in 2018 as a Bachelor Thesis project at the Max Planck Institute [1]. It used 10 PIN diodes as detector followed by an amplifier circuit. The board consisted of three such circuits with three different concepts for amplifiers for identifying the best among the three. Figure 3 shown below depicts the Silex version 1 board.

The first circuit uses an amplifier with JFET which was developed together with Prof. Michael Bantel. This circuit gives the best output when one or two diodes are being used. As the number of diodes increases to 10, the performance degrades due to loading effects, i.e. it cannot be used for the amplification of signals from a larger number of diodes. The circuit would work fine if each of the diodes had a separate JFET, which, however, would make the circuit complicated and more expensive [21]

The second circuit used a charge sensitive amplifier using the JFET in a bootstrap [13] [14] configuration. This circuit was adapted from the application examples for the LTC6244 IC[13] and proved to work well with a large number of diodes. The third circuit consists of an amplifier without any JFET, but the output was not satisfactory. Hence the second circuit was identified to be the best among the three circuits, which is further used in the version 2 and version 3 board design.

The main drawback of this board was that there were only a small number of diodes used and thus the effective area of detection was small. These drawbacks were resolved in the next version of the board.

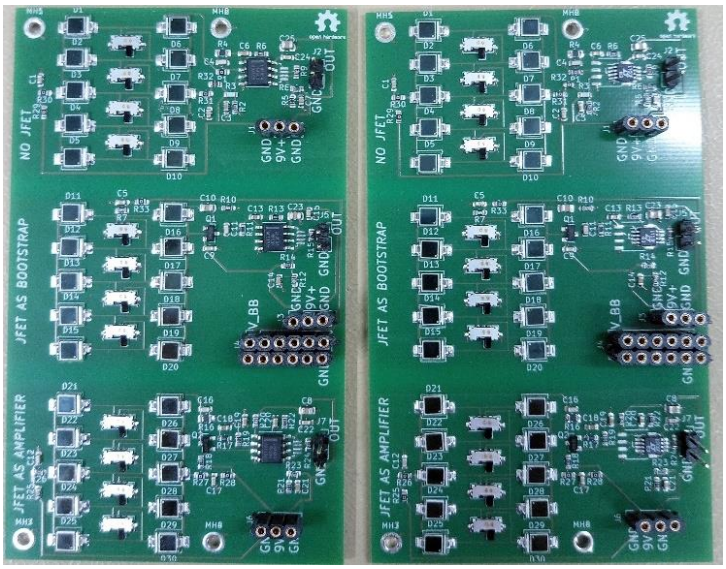

Fig 4. Version 1 Board

4.2 Silex Version 2 Board

The second version of the boards was designed in the year 2019 and had a major improvement in the output signals. The version 2 board consists of up to 50 diodes followed by an amplifier circuit. It also incorporated the bootstrap amplifier as a charge sensitive amplifier from the version 1 board which gave good results. The amplifier part of the circuit includes a JFET and two-amplifier stages which in turn are responsible for the good output signals. The version 2 board consists of a top board and a bottom board to check for coincidences in the output signals. The top board and the bottom board use the same circuit, placed such that the diodes in the top board and the bottom board will be facing each other exactly in order to do the coincidence measurement.

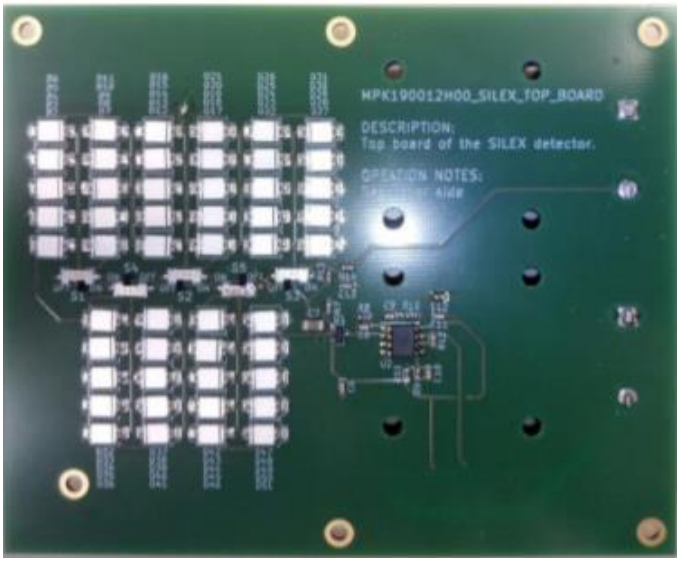

Fig 5. Top board of version 2 Board

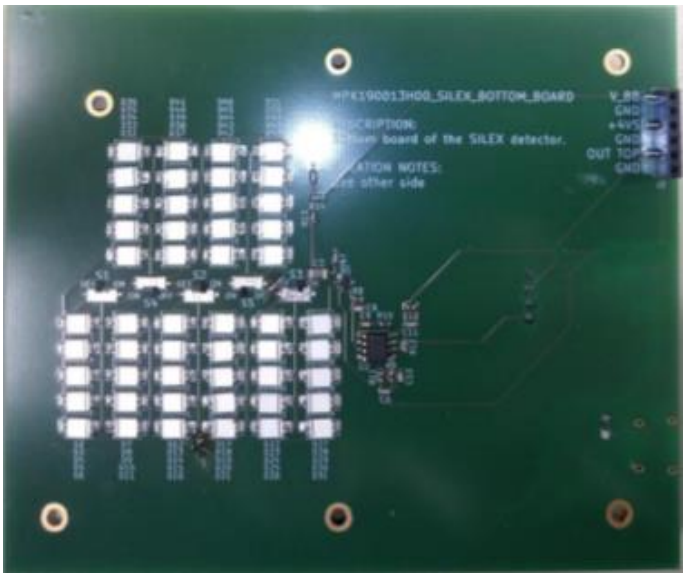

Fig 6. Bottom Board of version 2 Board

The initial testing within the work leading to this Master Thesis began with this version 2 board and the changes made were incorporated into the design of the version 3 board. The main drawbacks of the version 2 board was a tendency for oscillations and large low-frequency noise components in the output signals. The signal and noise were not well distinguishable in this version, which was to be resolved in the version 3 board. The various changes that are incorporated in order to resolve these drawbacks are elaborated in the following chapters.

4.3 Modifications to Version 2 Board

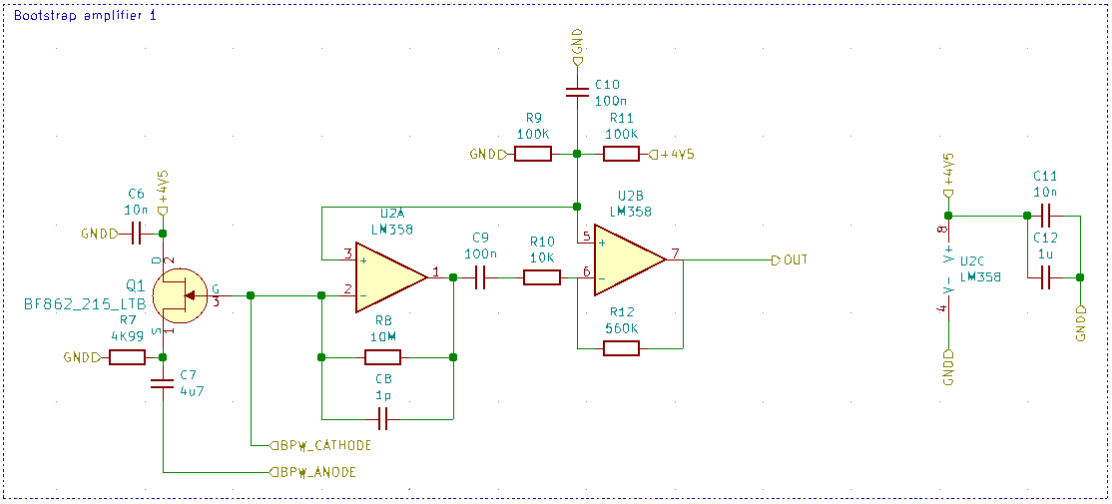

Fig 7. Amplifier Sheet for bottom board of Silex version 2 board

Initially, the output signals of the version 2 boards (circuit in appendix) contained oscillations, which was resolved by changing the resistor and capacitor (C8, R8), in the feedback loop of the first amplifier stage to 10MOhm and 6.8pF, as was used in the version 1 board. The output thus obtained didn't have any more oscillations and gave a reasonable signal. The main drawback faced at this point was a large noise contribution in the low frequency region. The next change made in this board was that the resistor and capacitor between the anode and JFET was changed to 1 uF(C13) and 500 Ohm(R14) respectively (in the diode sheet for version 2 board schematics). This change made the diode less susceptible to outside noise and as well helped in buffering the batteries, which are used to supply the bias voltage. During this Thesis, these changes were incorporated into and tested with the given circuit. The various modifications and changes that were made to the version 2 board and which were to be incorporated into the version 3 board are as follows

a. Addition of a voltage regulator
b. Addition of a high-pass filter

c. Addition of impedance decoupling
d. Replacing the LM358 amplifier with the AD823 amplifier

4.3.1 Addition of a voltage regulator

The voltage required to drive all the elements in the entire circuit board was chosen to be 4.5V. In order to stabilise the entire circuit, the initial modification was the addition of a linear regulator to the circuit. For the version 2 board the voltage regulator was connected externally.

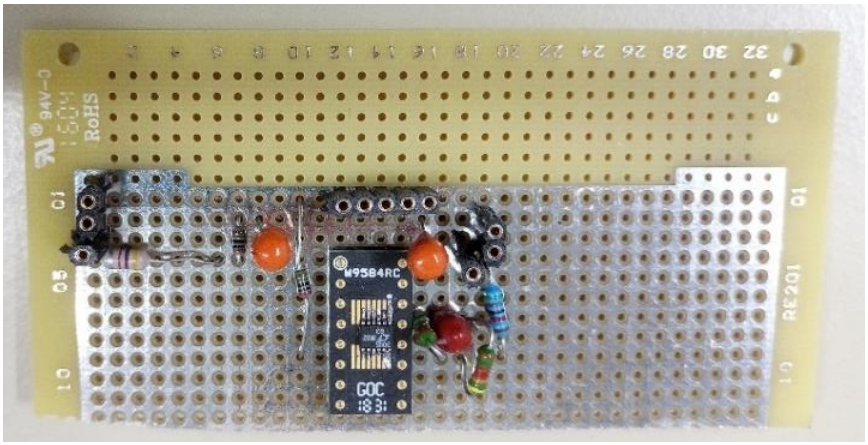

Fig 8. Voltage regulator circuit implemented on bread board

The voltage regulator used is the LT3045 IC, which is a low-cost, low-noise and low dropout linear regulator. The regulator converts the 9V input supplied by the battery to 4.5 V which ensures safe functioning of the board and is at the same time compatible with the use of USB power, as foreseen for the final system. Initially, the entire circuitry for the regulator was realized on a bread board, which was then connected to the power pin of the version 2 board using wires as shown in Figure 8.

Figure 9. Shows the output signal of the version 2 board with the voltage regulator added. The circuit shows no oscillations at the output but contains significant noise.

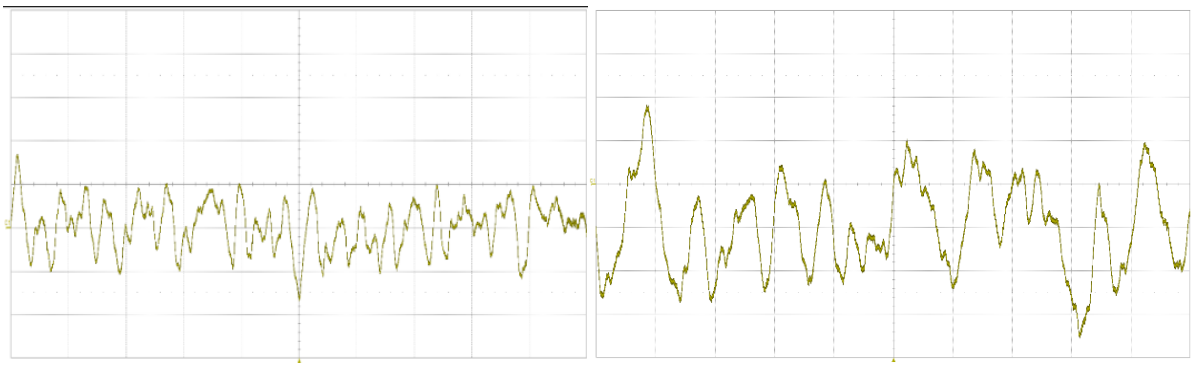

(a) (b)

Fig 9. Output signal of (a) top board with regulator *[X-axis = 200us/div and Y-axis = 20mV/div]* (b) Bottom board with regulator *[X-axis = 100us/div and Y-axis= 50mV/div]*

Considering the output signal of the bottom board, the noise seems to be much higher than that in top board. This was an early test done in the initial stage. Taking the spectrum of the output, a large amount of low-frequency noise was observed, which is to be reduced by adding a high-pass filter to the output.

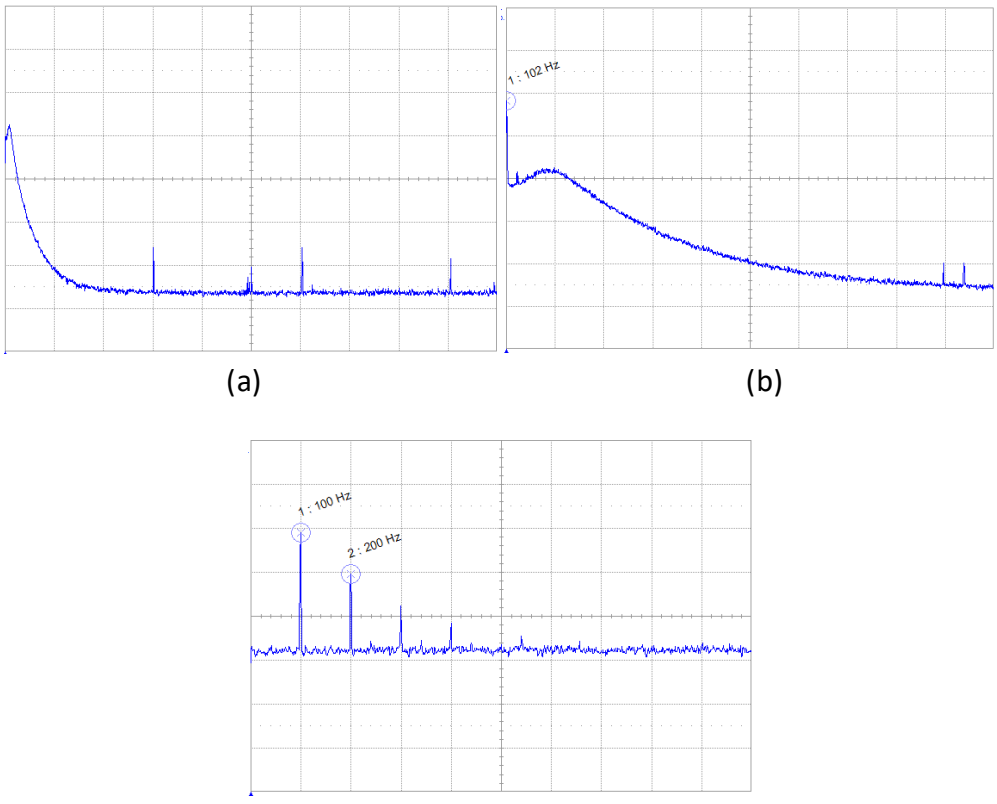

(a) (b)

(c)

Figure 10. Spectrum (FFT) for the output of Silex version 2 board with regulator with Y-axis 10 dB/div and X-axis having a span of (a) 1MHz (b) 100KHz (c) 1KHz

In Figure 10. (a), the graph shows the spectrum of the output signal for a frequency of 1MHz. In the lower frequency range, the spectrum has quite a large

value of about 40dB which later on drops as the frequency increases. This depicts the noise. Looking into the spectrum for 100KHz, we can view a similar pattern for the spectrum where it reduces with frequency from approximately 30dB. A reduction in the noise level can be observed below 10Khz in Figure 10 (b). This is because the resistor and capacitor pair (C9 and R10) functions as a filter which thereby reduces the noise levels. Further looking into the spectrum for 1KHz, the signal contains harmonics at 100Hz and 200Hz. This is caused when ambient light penetrates through gaps in the enclosure and reaches the PIN-diode and produces peaks or harmonics at regular intervals. This, in turn cements the need for low-frequency noise filtering in the circuit and a light-tight enclosure.

4.3.2 Addition of a high-pass filter

The low frequency noise in the output signal was the major drawback to Silex version 2 board. In order to remove the low-frequency noise, a high-pass filter circuit was added on to the board. The output of the second amplifier stage was fed as the input to the filter circuit. The filter circuit was also implemented on a bread board and the output of the version 2 board was supplied to the input of the filter circuit on the bread board via connectors. The figure below (Figure 11) shows the circuit used.

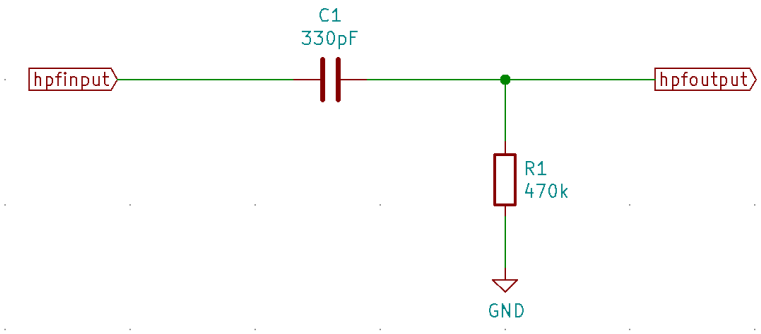

Fig 11. Circuit for high-pass filter

The high-pass filter values were set by testing the output with a high impedance high-pass filter (470 K Ohm and 330pF) as well as with a low impedance high-pass filter (470 Ohm and 330nF).

The resistor and capacitor values were set according to the following formula.

$$F_c = \frac{1}{2\pi R_1 C_1}$$

Since the output signals are approximately in the range of 10 KHz and we need to filter out the low frequency signals below 1 KHz, the frequency F_c was chosen to be 1KHz, which is sufficiently far away from the frequency range of the signals. For a high-impedance high-pass filter, the resistor was chosen as R = 470 KOhm. The requirement F_c = 1 KHz then determines the capacitor to have

$$C_1 = \frac{1}{2\Pi R_1 F_c} = \frac{1}{2*3.14*470*10^3*1*10^3}$$

$$C_1 = 3.387*10^{-10} = 338.7*10^{-12} = 330pF$$

Similarly, the resistance and capacitance for a low impedance high-pass filter was fixed to R = 470 Ohm and C = 330nF.

The different combinations of filters tested were: single high impedance high-pass filter, single low impedance high-pass filter, two high impedance high-pass filters in series and two low impedance high-pass filter in series. The results obtained were as follows.

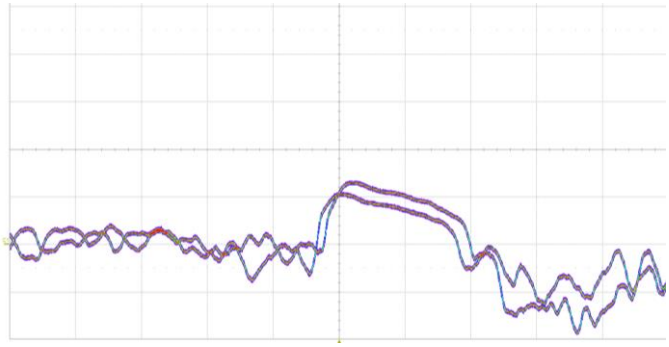

Fig 12. Output signals of version 2 board with single low impedance high-pass filter in persistence mode *[Y-axis = 100mV/div and X-axis = 100µs/div]*

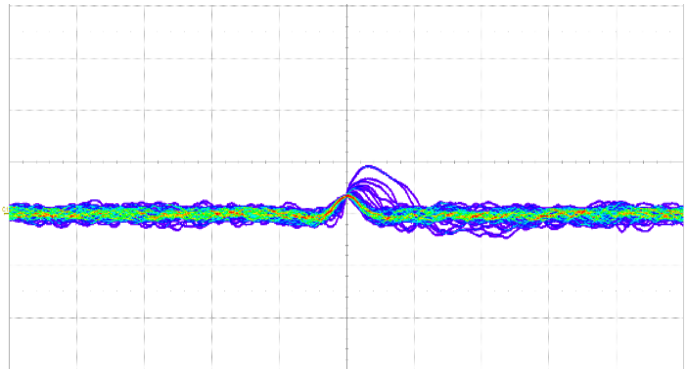

Fig 13. Output signals of version 2 board with two low impedance high-pass filter in persistence mode *[Y-axis = 100mV/div and X-axis = 100µs/div]*

The low impedance high-pass filter used C1 = 330nF and R1= 470 Ohm. It is observed that the signal quality degrades when this low impedance high-pass filter is used to filter out the low frequency noise components (Figure 12.). It can also be observed that the separation of the signal from the noise component is not that good, and hence that the signal quality degrades. Further, using two low impedance high-pass filters also doesn't make a significant difference in the signal quality. This is because the second high-pass filter acts as a load to the first high-pass filter. Looking into Figure 12 and 13, it is observed that the signal quality degrades considerably when using low-impedance high-pass filters. Hence, the conclusion is that a low-impedance high-pass filter is not a good option to remove the low-frequency noise components from the output signals of the detector.

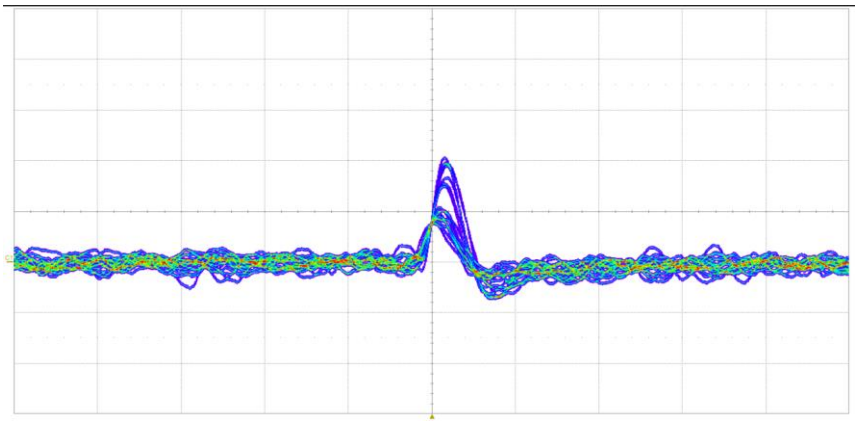

Fig 14. Output signals of version 2 board with single high impedance high-pass filter in persistence mode *[Y-axis = 50mV/div and X-axis = 100µs/div]*

For the high impedance high-pass filter, R1 was replaced with a 470 KOhm resistor and the capacitance (C1) was adjusted accordingly to 330pF.

Figure 14 shows the output signals in persistence mode run over 10 minutes when a single high impedance high-pass filter is used. It can be observed from Figure 14 that the signal quality is much better than that for a low-impedance filter. The filter retains the shape of the signal and as well gives reasonable output signals. The noise and the signal components are quite distinguishable.

Figure 15 shows the spectrum for the same output signal over different frequency ranges.

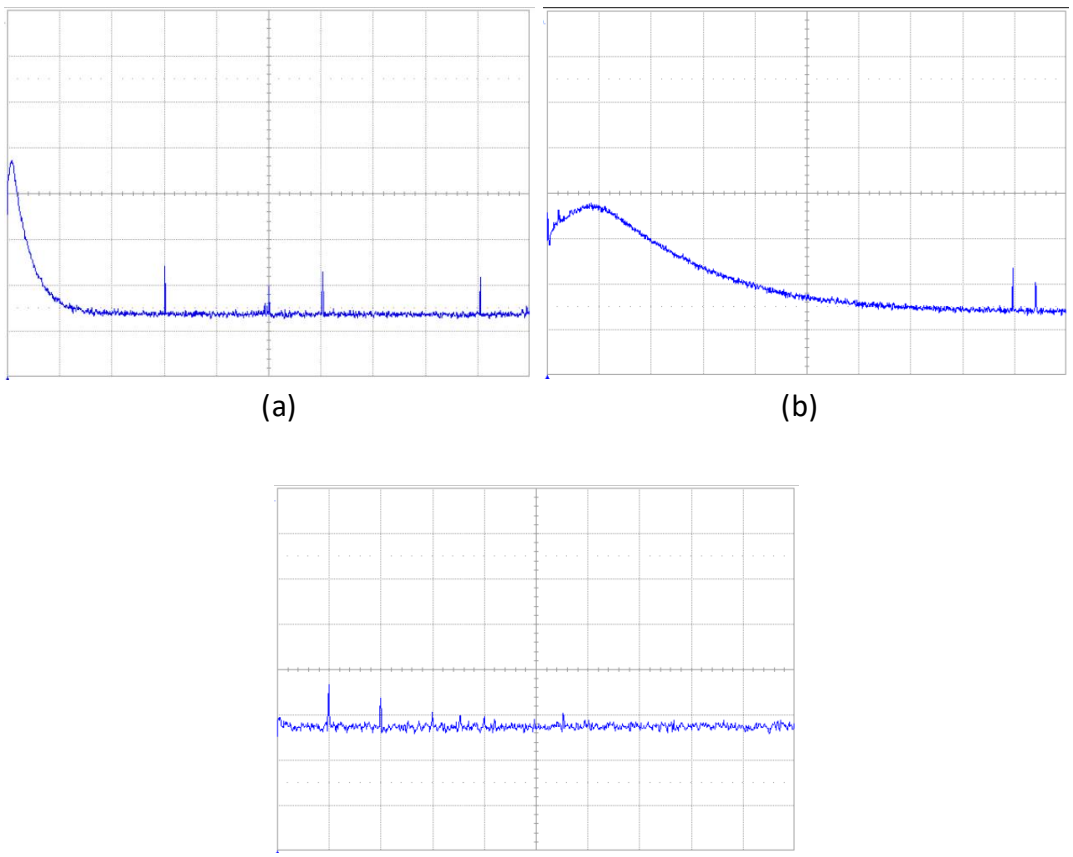

(a) (b)

(c)

Fig 15. FFT for output signal with single high impedance high-pass filter having Y-axis with 10dB/div and X-axis having a span of (a) 1MHz (b) 100KHz (c) 1 KHz

From Figure 15. (a), the noise signal is reduced by about 10dB in the low-frequency range, which is 10 times less than the noise in the circuit without any

filters. Frame (b) shows the FFT of the output signal for the frequency range of 100 KHz and we can observe that the low frequency noises have been considerably reduced. Further looking into Figure 15. (c), the harmonic components of oscillation have also significantly reduced. It thus proves to be the preferred method to remove the low frequency noise while retaining signal quality.

The final batch of tests for filters were conducted with two high impedance high pass filter in series. Figure 16 shows the output waveforms with two high impedance high-pass filters in persistence mode run over a time interval of about 10 to 15 minutes.

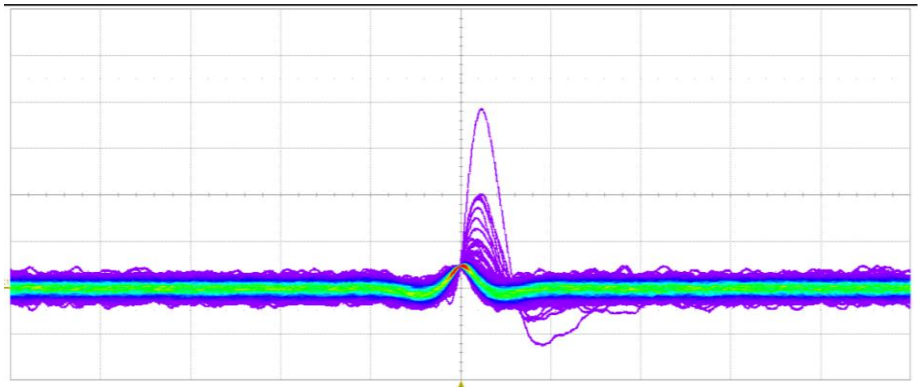

Fig 16. Output signals with of version 2 board with two high impedance high-pass filter in persistence mode *[Y-axis = 50mV/div and X-axis = 100µs]*

It can be observed that the output signal is more suppressed though the signal shape is maintained when compared with the output signals of the circuit with a single high impedance high-pass filter. It has better signal quality than that of low impedance filters, but less than that with a single high impedance high-pass filter. Moreover, the second high-pass filter acts as a load to first high-pass filter and thereby, the output signals are suppressed. From this plot, the noise looks almost similar to the previous one (Figure 14.). To further check the noise levels in the circuit, the spectrum of the output signals can be analysed.

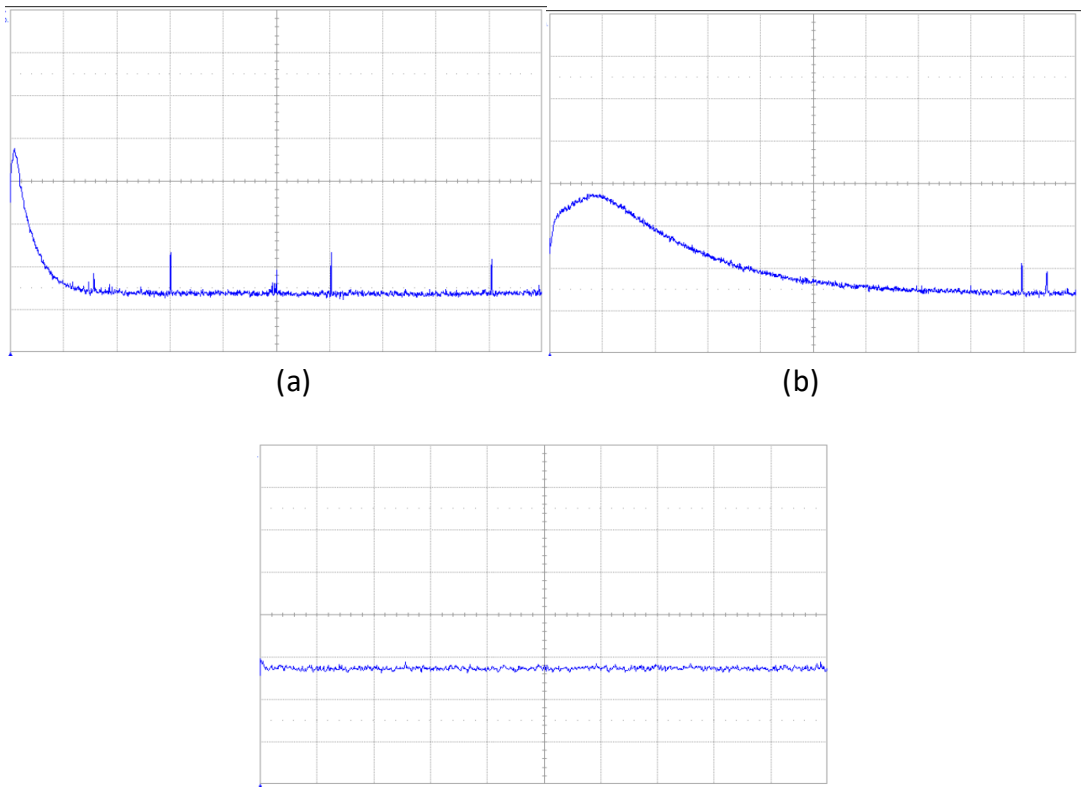

(a) (b)

(c)

Fig 17. FFT for output signal with two high impedance high-pass filter having Y-axis with 10dB/div and X-axis having a span of (a) 1MHz (b) 100KHz (c) 1 KHz

It can be observed from the FFT graphs of the filter (Figure 17) that there is a significant reduction in the low frequency noise. There is almost no spikes (harmonics) in the lower frequencies as seen in Figure 17 (c). Taking a closer look at the low frequency ranges in graph Figure 17 (a) and (b), the reduction in the low-frequency noise is quite evident and is almost similar to that with a single high impedance high-pass filter. But the output signal is more suppressed than that of the single high impedance high-pass filter.

So, comparing all four combinations of the filters, it is evident that a high impedance high-pass filter is best suited for this circuit. It is deduced that the low impedance high-pass filters reduce the signal quality considerably even though the noise levels are still high, indicating that the first amplifier stage is not able to drive a low-impedance load. High-impedance filters have better signal quality and significant reduction of noise signals in the low frequency

ranges. Considering, the two combinations of high-impedance filters, the noise is reduced significantly when using two high-impedance HPFs but the output signals are more suppressed, which in turn affects the signal quality. When considering only a single high-impedance filter, the output signals are better and the noise is also reduced significantly. There is no significant difference in the noise reduction when using a single high impedance high-pass filter and two high impedance high-pass filter. Therefore, a single high impedance high pass filter is decided to be used in further designs.

4.3.3 Addition of Impedance de-coupler

The main aim of adding this part is to transfer a voltage with high impedance output to a circuit with low impedance input. It essentially does impedance matching between two circuits. The outputs of the two boards need to be supplied to a microcontroller unit in order to do the further manipulations required to display the output in a user-friendly format. The ADC of the chosen [18] microcontroller however has an input impedance of about only 2 KOhm. Hence, impedance matching is crucial. It makes sure that the signal source, i.e. the boards are prevented from being affected by whatever currents that the load at the ADC may produce. The figure below shows the circuit for the impedance de-coupler added after the filter. Here, an additional resistor R2 was also added as a pull-up resistor. As a consequence, the central frequency F_c changes to 2KHz which is still sufficiently far away from the frequency range of the signals and thus does not affect the resulting signals.

We use a voltage buffer amplifier or voltage follower for this purpose as seen in Figure 18. A voltage buffer amplifier has a high input impedance and a low output impedance and has unit gain, which in turn makes sure that the output

voltage remains the same. It thus serves the purpose of impedance matching between the boards and the microcontroller.

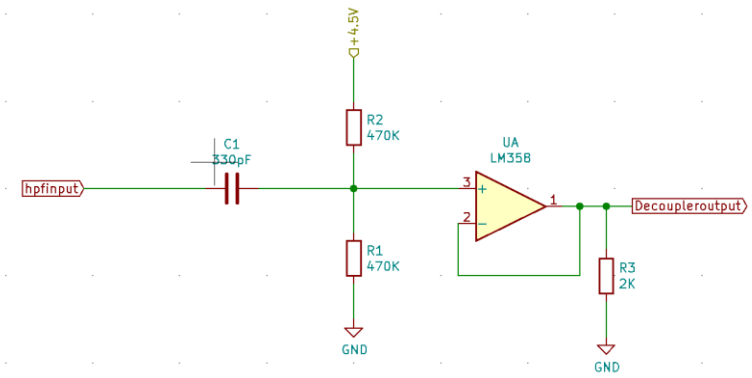

Fig 18. Circuit diagram for high-pass filter followed by Impedance de-coupler

The output signal when using an inverting op-amp as a buffer is shown in the figure. In order to check if the circuit works fine, initially the input was supplied by a function generator.

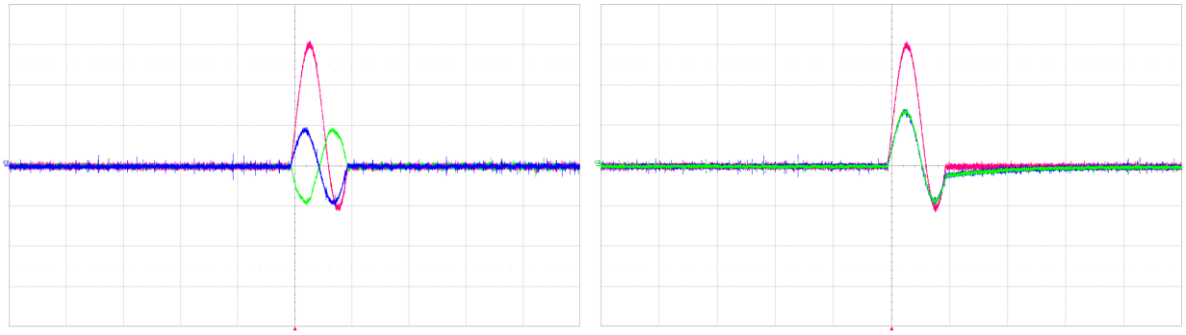

(a) (b)

Fig 19. Output signals of version 2 board using (a)inverting amplifier as buffer (b)non-inverting amplifier as buffer *[Y-axis = 50mV/div and X-axis = 100µs/div]*

A single pulse of sine wave was given as input to the circuit which is represented as the pink graph in Figure 19, (a) and (b). The blue line shows the output of the filter and the green line shows the output from the de-coupler. The addition of the filter suppresses the input signal as is seen in the analysis before. It is observed that both the inverting amplifier and the non-inverting amplifier qualitatively work well. Taking a closer look at the two graphs, the output signal

with the filter and non-inverting amplifier as a buffer tends to suppress the signal more. The output signal of the non-inverting amplifier is approximately 25mV higher than that of the inverting amplifier which is about a 50% increase in signal strength. It can thus be concluded that the type of amplifier used i.e., whether the amplifier used is inverting or non-inverting, plays a significant role in the signal quality. The non-inverting amplifier as a buffer was selected for further testing. The circuit was then supplied with the output of version 2 boards as input.

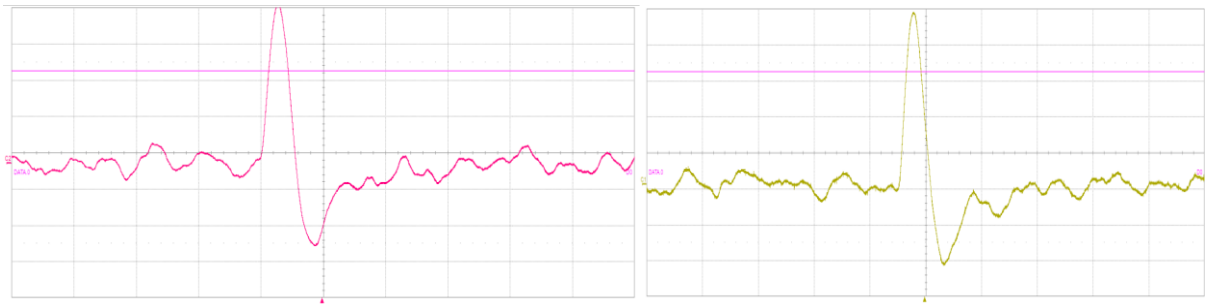

(a) (b)

Fig 20. Output signal of version 2 board with filter and decoupler (a) top board (b) Bottom board *[Y-axis = 50mV/div and X-axis = 100µs/div]*

Figure 20 shows the output signals with filter and de-coupler to the top board (a) and the bottom board (b) with the trigger applied for the top board and bottom board respectively in order to compare genuine output signals. Figure 21 shows the same outputs in persistence mode run over approximately 10 minutes.

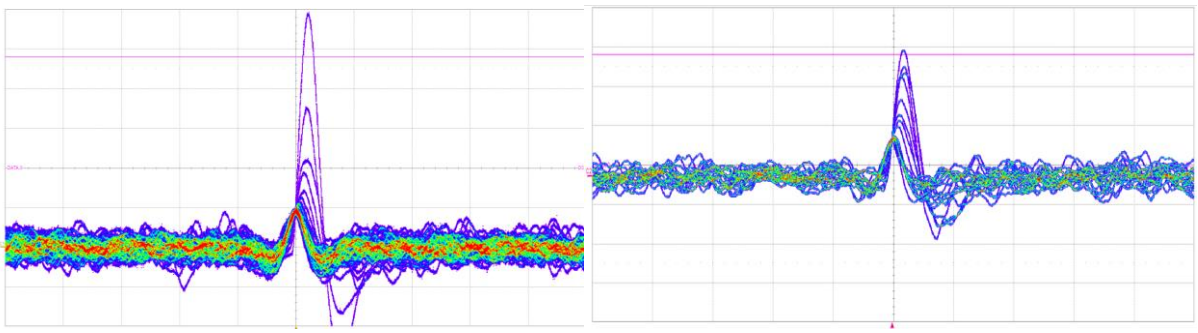

(a) (b)

Fig 21. Output signal of version 2 board with filter and decoupler in persistence mode (a) top board (b) Bottom board *[Y-axis = 50mV/div and X-axis = 100µs/div]*

It can be observed that the circuit works well and there is no degradation of the signal as the voltage follower doesn't affect the output signals of the filter as it has unity gain.

To further analyse the noise levels and the signal, the FFT of the output was taken. The figure below shows the spectrum of the output signals taken over the frequency range of 1MHz, 100Khz and 1Khz

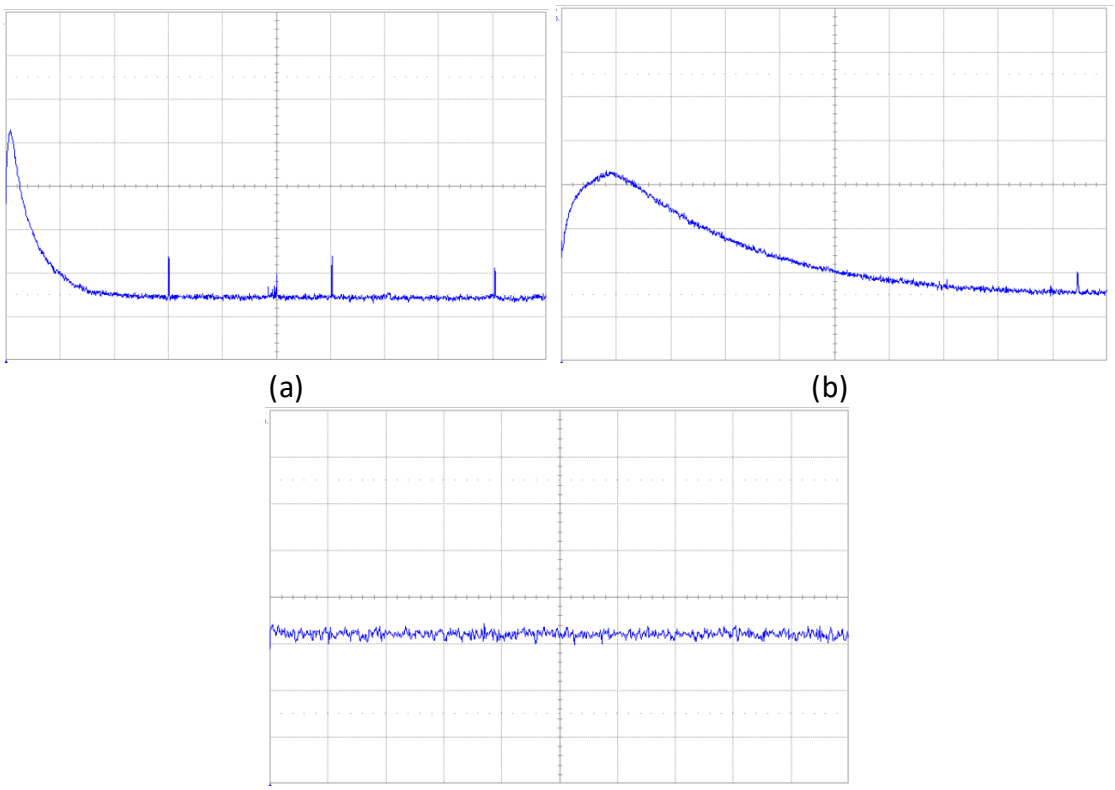

Fig 22. FFT for output signal for version 2 board with high impedance high-pass filter and non-inverting amplifier as de-coupler having Y-axis with 10dB/div and X-axis having a span of (a) 1MHz (b) 100KHz (c) 1 KHz

It can be seen from Figure 22 that the output signals are very good. The harmonics that were present in the low frequency ranges were completely removed and the signals are much better. The circuit with all modifications added proves to be good.

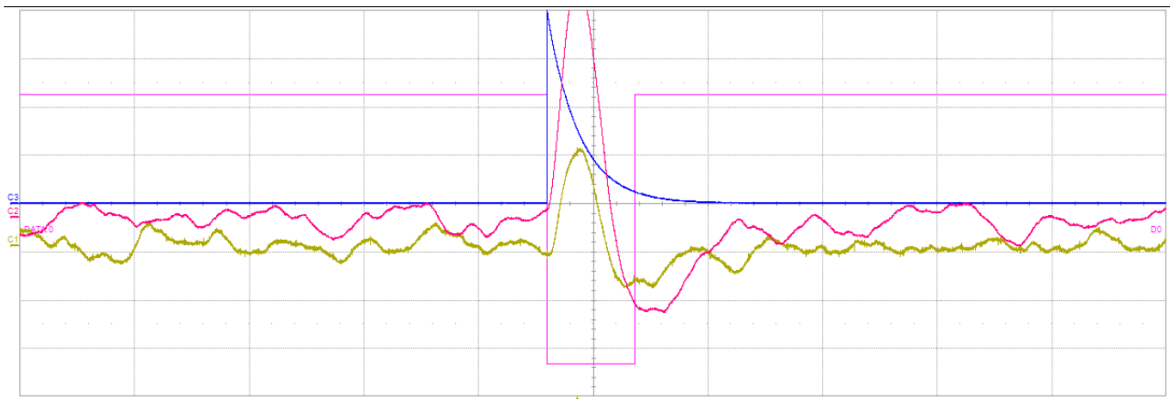

Fig 23. Graph showing coincidence between top board (red), bottom board (yellow) and Cosmo detector (pink and blue) with trigger on bottom board
[X-axis = 100us/div and Y-axis = 50mV/div]

A coincidence measurement between top board, bottom board and the Cosmo detector is shown in Figure 23. The red line shows the waveform for the top board, yellow line shows the waveform for bottom board and the blue line and pink line shows the Cosmo detector signal in analog and digital form, respectively. A trigger is supplied from the oscilloscope to channel 1 i.e. the bottom board. A coincidence means that there is a signal generated in the top board, bottom board and the Cosmo detector which implies that a particle was observed in all the 3 detectors.

4.3.4 Replacing the LM358 amplifier with an AD823 amplifier

All testing till now was done with the LM358 operational amplifier in the first stage. Looking into the data sheet of the LM358, it is observed that the input voltage range of the LM358 is,

V_{in} = 0 to (V_{supply} – 1.5V)

= 0 to (4.5V – 1.5V)

= 0 to 3 V

In our case, the supply voltage is 4.5V, so the voltage range of LM358 is limited to 0 to 3V. If the signal goes above 3V, then the output signal will be clipped or

distorted. So, there is a voltage limit when using the LM358. In the future, the addition of a microcontroller-based readout system is planned. Since the Atmel SAM E54 is already in use within the division, it is currently favoured as the best option for this purpose. The microcontroller has an Internal ADC which can use an internal and external reference voltage. A voltage range of 0 to 3.3V decreases the resolution when using an ADC. So, to increase the resolution and to account for a better rail-to-rail amplification, a different op-amp with a wider range was sought. A candidate replacement for the LM358 was the AD8628/29 which has a good rail-to-rail amplification. For a voltage supply of 0 to 5V, the output voltage can go from 0 to 4.5V. The AD8628 contains a single op-amp where as AD8629 consists of a dual op-amp enclosed in a single package. Since the amplifier used in the circuit has two amplification stages and the AD8629ARZ costs around 2 Euros it is a good low-cost substitute for the LM358.

Initially, the new op-amp was tested on the version 1 board. The LM358 was replaced with the AD8629 in the version 1 board and the figure below shows the output signals.

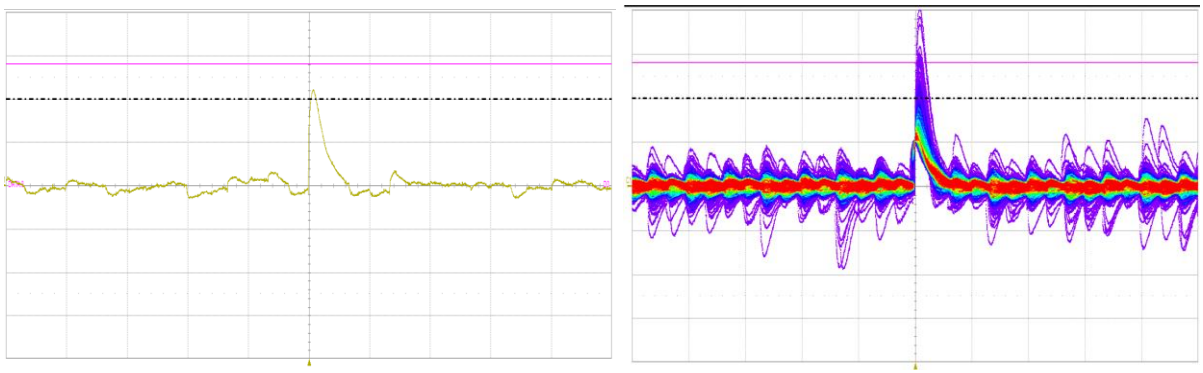

(a) (b)

Fig 24. Output signals for version 1 board with LM358 replaced with AD8629 *[X-axis = 50us/div and Y-axis = 50mV/div]*

It can be observed from Figure 24 that the output signals are of poor quality. There seem to be oscillations as well as high noise levels in the output signals. Using AD8629ARZ instead of LM358 seriously degraded the output signal

quality. Therefore, using AD8629ARZ proved to be a poor choice for this circuit. Another low-cost and dual op-amp substitute suggested was the AD823. The AD823 also has a high input impedance as it has a FET input. The output voltage for the AD823 goes very close to the rail voltages. If the supply voltage is 5V, the output voltage can go to nearly 4.95V, i.e. really close to the supply voltage. So, the version 1 board was tested with the new AD823 instead of LM358. The figure below shows the output waveform thus obtained.

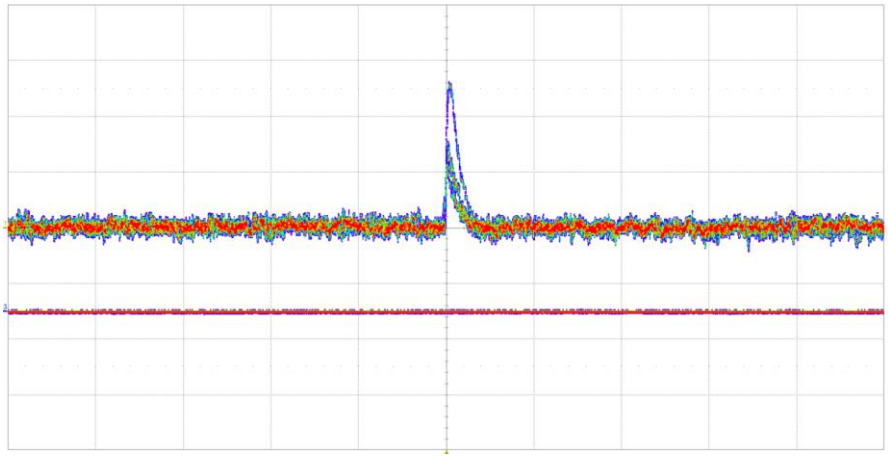

Fig 25. Output signal of version 1 board with LM358 replaced with AD823 *[X-axis = 100us/div and Y-axis = 20mV/div]*

Figure 25 shows the output signal in persistence mode taken over about 5 minutes. It can be seen from the waveform that the output has good signal quality and that signal and noise are clearly distinguishable. The new AD823 hence proved to be a good substitute for LM358. The version 2 boards were then tested with the new AD823 IC and the results are then studied.

Figure 26 shows the output signal of the version 2 board with the LM358 replaced with the AD823 in persistence mode run over an interval of about 10 minutes. It can be observed that the version 2 boards also give a reasonable output when using AD823 instead of the LM358. The circuit was tested with different values of resistor-capacitor combinations in the feedback loop as depicted in Figure 25 (a) and (b).

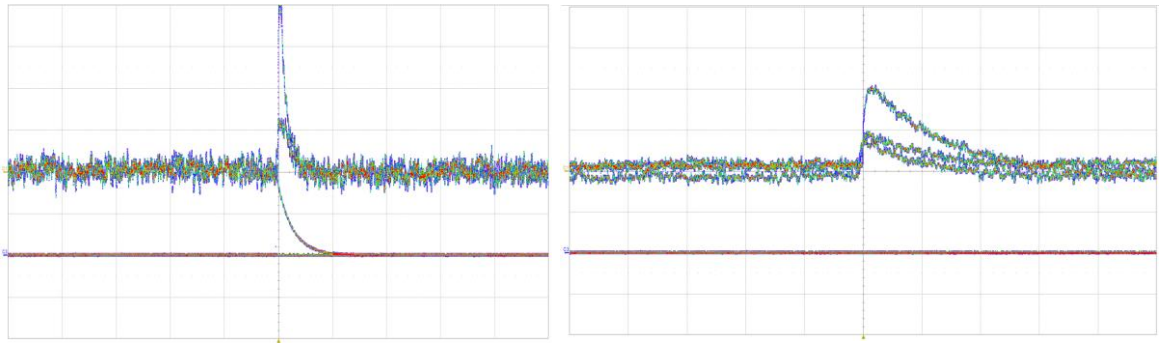

(a) (b)

Fig 26. Output signals for version 2 board and Cosmo detector with LM358 replaced with AD823 and (a) 1M resistance and 15pF capacitance in the feedback loop *[X-axis = 100us/div Y-axis = 20mV/div]* (b) 10M resistance and 15pF capacitance in the feedback loop *[X-axis = 100us/div Y-axis = 50mV/div]*

Looking closer into the graphs, the output signals when using 1M and 15pF goes to about 80mV when run over an interval of 10 minutes and has higher noise. The decay time of the output signal in Figure 26(a) is given by

$\tau = RC$

$= (1*10^{6}) * (15*10^{-12})$ s

$= 15$ µs

When using 10M and 15pF in the feedback loop, the output signal goes to about 100mV. The decay time from the graph is slightly more than that calculated but not significantly different. It can be observed that the output signals have higher voltages when using 10M and 15pF than 1M and 15pF in the feedback loop of the amplifier. The noise is also low in this configuration. The decay time of the output signal in Figure 26(b) is given by

$\tau = RC$

$= (10*10^{6}) * (15*10^{-12})$ s

$= 150$ µs

The output signals are significantly longer and wider with the 10M and 15pF in the feedback loop. The testing of the new op-amp done so far did not use any

filter circuit and impedance decoupling circuits. The next set of tests were done with the filter and de-coupler stages.

4.4 Version 2 Board with AD823, Voltage regulator, filter and impedance decoupler

The entire set up of the version 2 board with all the modifications is shown in Figure 27. The high-pass filter circuit and the impedance decoupling circuit which was tested previously was added on to the version 2 board as external circuitry. A piece of aluminium foil covered with plastic was placed in between the two boards one time, as there seemed to be some cross-talk due to capacitive coupling. The foils were later removed as we concluded from the analysis of the data that the small cross-talk between the two boards only marginally affected the results.

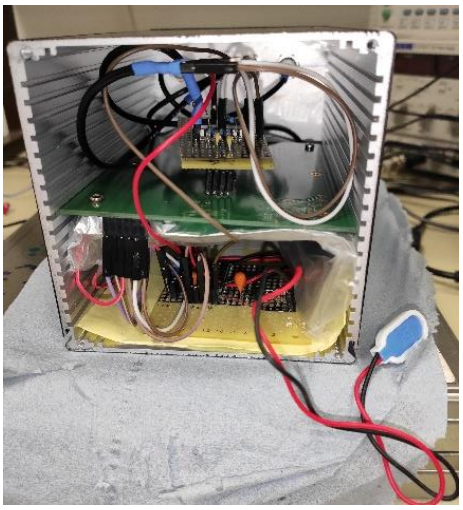

Fig 27. Version 2 board set up with all modifications.

The bread board on the top of the version2 board is the filter and de-coupler circuit and the one in the bottom is the voltage regulator. In addition to these, two batteries to bias the diodes as well as a 9V battery as power supply were connected and placed inside the enclosure before taking the readings. It can be seen that the entire set up is quite untidy. The outputs were tested with

different combinations of resistor and capacitor in the feedback loop of the amplifier (C8 and R8) and the resulting outputs are shown below.

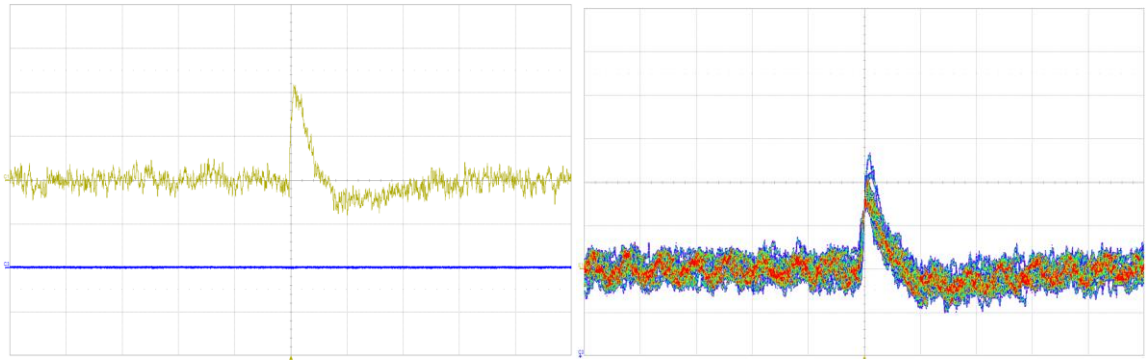

(a) (b)

Fig 28. Output signals of version 2 board with filter, impedance decoupler and LM358 replaced with AD823 with 10M resistance and 6.8pF capacitance in the feedback loop *[X-axis= 100us/div and Y-axis = 50mV/div]* (a) Output signal (b) Output signal in persistence mode

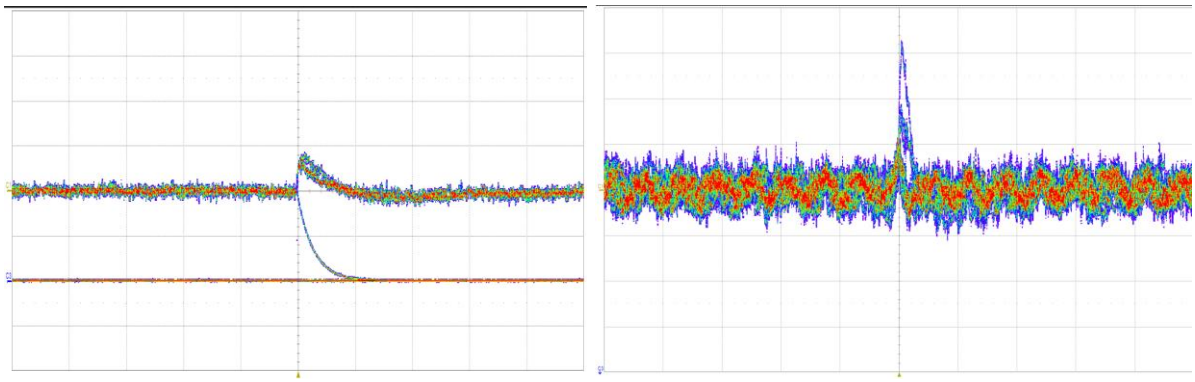

(a) (b)

Fig 29. Output signals of version 2 board with filter, impedance decoupler and LM358 replaced with AD823 in persistence mode with (a) 10M resistance and 15pF capacitance in the feedback loop *[X-axis = 100us/div and Y-axis = 50mV/div]* (b) 1M resistance and 25pF capacitance in the feedback loop *[X-axis = 100us/div and Y-axis = 20mV/div]*

Figure 28 and 29 shows output signals of version 2 board with LM358 replaced by the AD823 and filter as well as impedance de-coupler circuit. The testing is done using three different capacitance and resistance combinations in the feedback loop of the amplifier (R8, C8) – 10 MOhm and 6.8 pF (decay time, τ= RC = 68 µs), 10 MOhm and 15 pF (decay time, τ= RC = 150 µs) and 1 MOhm and 25 pF (decay time, τ= RC = 25 µs). Figure 28 shows the output signals with 10MOhm and 6.8 pF in the feedback loop of the amplifier. It can be observed

that we get reasonable output with an output signal of about 100mV. The noise signals and the output signals are distinguishable and the circuit works fine using this configuration, but there is still significant noise in the output.

Looking into the output waveforms obtained with 10MOhm resistance and 15pF capacitance in the feedback loop of the amplifier is used (Figure 29 (a)), the output signal is about 50mV when run in persistence mode for about 5 minutes. It can be observed that the noise level is much less than that with a 10 MOhm resistance and 6.8pF capacitance in the feedback loop. Presumably, higher signal values would have been visible using 10MOhm resistance and 15pF capacitance, if the output signals in persistence mode was run for a longer time.

It can be observed from Figure 29 (b) that the output signals are approximately equal to 50mV, when 1 MOhm resistance and 25pF capacitance is used in the feedback loop. The signal quality degrades and the noise is much higher when this configuration is used. From the above analysis, it can be concluded that 10MOhm and 15 pF resistance and capacitance in the feedback loop of amplifier has good signal quality as well as low noise level and 10MOhm and 6.8 pF resistance and capacitance in the feedback loop has high output signals as well as high noise, whereas 1MOhm and 25pF resistance and capacitance in the feedback loop degrades the signal quality with higher noise levels. Hence the coincidence measurement was carried for Silex version 2 board using 10MOhm and 15pF in the feedback loop.

4.5 Calculations

a) Energy loss, primary charge and photodiode data

These calculations give an approximate idea of the expected output signal. The main source of energy loss for a muon that is passing through matter is ionisation. The minimum energy loss in silicon is given by

E_{loss} = 1.66 MeV/(g/cm^2)

The density of Silicon, ρ_{si} = 2.33 g/cm^3 and thickness d = 0.01 cm (which was measured)

The energy that is available to create electron- hole pairs is given by,

$E_{deposit}$ = 1.66 MeV/(g/cm^2) * 2.33 g/cm^3 * 0.01 cm

= 38.678 keV

The energy required to create an electron – hole pair in Silicon is approximately 3.6 eV. Therefore, a muon passing through 100 µm of Silicon will create a measurable charge of approximately 11000 electrons.

The charge, Q = 11000 * 1.6*10^{-19}

= 1.76 * 10^{-15} C

The capacitor that is used in the amplifier stage is selected to be 15pF in the version 2 board. Hence, the voltage V is

$V_{15pF} = \frac{Q}{C} = \frac{1{\cdot}76*10^{-15}}{15*10^{-12}}$ *= 0.14 mV.*

The board was also tested with 10pF and 6.8pF in the feedback loop and the voltages are given as

$V_{10pF} = \frac{Q}{C} = \frac{1{\cdot}76*10^{-15}}{10*10^{-12}}$ *= 0.17 mV.*

$V_{6.8pF} = \frac{Q}{C} = \frac{1{\cdot}76*10^{-15}}{6.8*10^{-12}}$ *= 0.25 mV.*

When this signal passes through the second amplifier stage which has a gain of 56, the total voltage

V_{15pF} = 0.14 * 56

= 8.2 mV.

V_{10pF} = 0.17 * 56

= 9.52 mV.

$V_{6.8pF}$ = 0.25 * 56

= 14 mV.

The expected output voltage of version 2 board with 15pF capacitance in the output is about 8.2mV. From Figure 29 (a), the output signal is about 50mV for version 2 board with 10MOhm and 15pF in the feedback loop. This is much more than the expected output signal. The output signal varies due to fluctuations in the energy loss. To obtain the graph, a trigger was applied to the board, which was set to select large signals and there are also signals not associated to muons, which tends to be larger than genuine muon signals like alpha decays from radioactive contaminations in the diode material.

b) Rise time

Rise time is defined as the time taken by a signal to rise from 10% to 90% of the signal peak. To calculate the rise time, the averaged and normalised signal obtained from the coincidence measurement is considered and is show in Figure 30.[22]

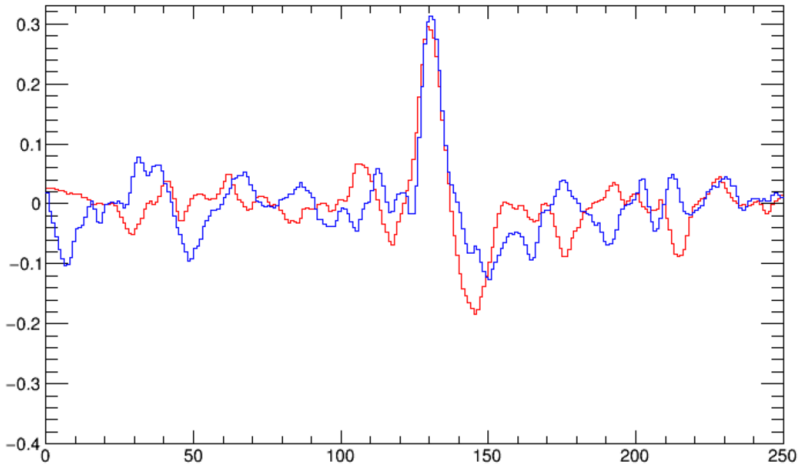

Fig 30. Averaged and normalised signal for version 2 board [22]

The x-axis consists of 250 samples, which is equal to a total span of 1ms. The time duration for one sample is

T = 1ms/250

= 4µs

For the signal to rise from 10% to 90%, it takes approximately 3 to 4 samples. Therefore, consider the number of samples as 3.5. The rise time is obtained as

$T_{rise} = T_{10\%}$ to $T_{90\%}$

$T_{rise} = 3.5 * 4\mu s$

$= 14\mu s$

4.6 Silex Version 3 Board

The third version of the Silex detector was designed in the year 2020 as part of this Thesis and is the latest version of the boards which is currently under active testing. All modifications incorporated into version 2 board which were elaborated upon in the previous section along with other changes, improved the signal quality in this version of the board. The design of this board is explained in the next chapter.

CHAPTER 5
Version 3 Board Design

5.1 Block Diagram

The block diagram for the top board and the bottom board are shown below, in Figure 31 and 32. It can be observed that both the top board and bottom board are the same, except that there is an additional voltage regulator circuit in the bottom board and the top board has additional batteries to supply the bias voltage for the diodes on both the boards.

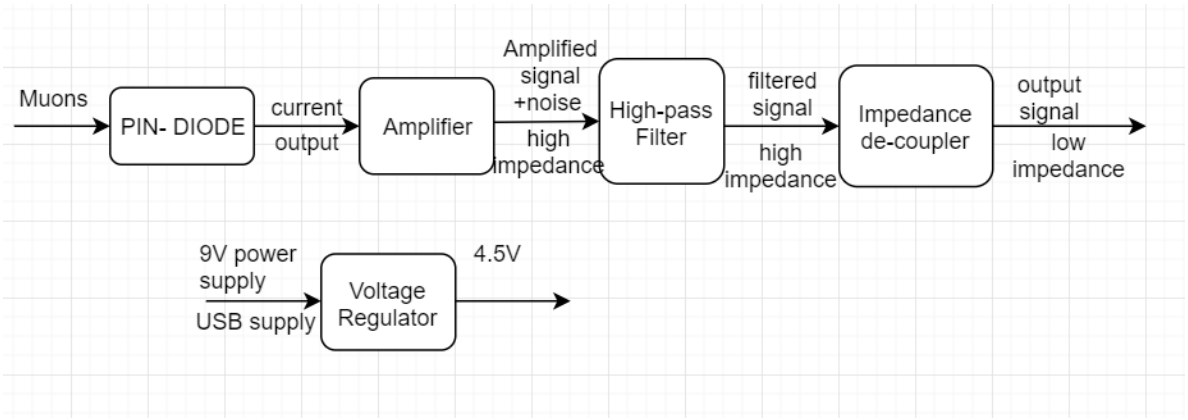

Fig 31. Block diagram for bottom board

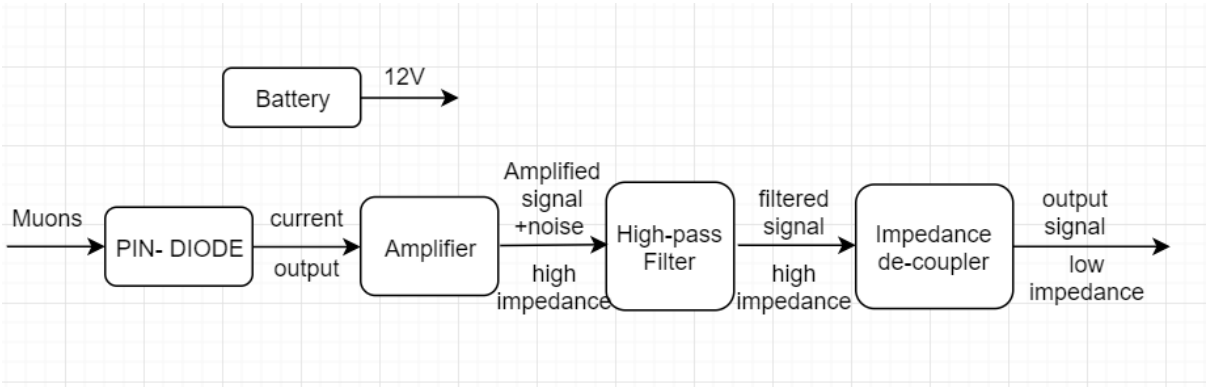

Fig 32. Block diagram for top board

The main parts of both the top board and the bottom board are the PIN-diodes, Amplifier circuit, high-pass filter and impedance de-coupler. These blocks were finalized after a series of tests that were conducted in the previous sections. In the block diagram for the bottom board of the Silex version 3 design (Figure 31),

the voltage regulator converts the 9V voltage supply from a battery down to 4.5V, which is required for the safe functioning of the boards. If a USB power supply is used, the voltage supply can be anywhere between 4.8V and 5.3V [19] [20] and hence, the use of a voltage regulator is essential in this case as well. The voltage regulator is responsible for supplying the 4.5V power to both the top board and the bottom board. The first main block in this design are the PIN-diodes. When a muon hits the PIN-Diodes, they generate charges which produce a current output. These output signals are then fed into an amplifier circuit which amplifies and gives measurable output voltage signals. The resulting amplified signals have high noise content in the low-frequency range as well as high impedance. The low frequency noise components are eliminated when fed into a high-pass filter. The output of the high-pass filter has high impedance and is then decoupled using an impedance de-coupler circuit to generate a low-impedance output signal, which matches the low-impedance input levels required by the ADC to be used.

The flow of the design for the top board (Fig 32) is the same as explained above. The bias voltages for the diodes were supplied using 12V batteries, which are added on the top board and then given to the bottom board though connectors. The next step in designing the version 3 board was implementing the circuit diagram corresponding to the block diagram. The design of the version 3 board was implemented using the software KiCAD [12] and is explained in the next section.

5.2 KiCAD

The entire design of the version 3 board was done using the software KiCAD, which is a free and open-source software used for electronic design automation (EDA). KiCAD facilitates the design of schematics (circuit diagram) for electronic circuits and can be used for its conversion into PCB layouts. KiCAD

also includes additional tools to create a bill of materials, artworks, Gerber files, and 3D views of the PCB and its components [12].

The flow chart illustrating the various steps involved in designing a printed circuit board using KiCAD is added in the appendix. The main steps involved in the designing are

a) Schematic

The first and foremost step is to draw the circuit diagram or the schematic. Once a project is created and opened, one can start drawing the circuit diagram in the schematic editor, 'Eeschema', in KiCAD. All the required components can be selected from the icon 'place symbol' in the toolbar. In case the components are not available, one can add the library for the required component by using the 'manage symbol libraries' button. The connections between the components can be created using the wire symbol available in the toolbar. Once the schematic is complete, the next step is to annotate the components.

b) Annotation

All the components that are used in the circuit should be named appropriately and should have unique identifiers. This step can be done automatically in KiCAD using the 'annotate schematic symbols' icon in the toolbar. It automatically assigns numbering for all the components while making sure that there is no repetition and hence makes it easier to identify all the components. Lastly one checks for any errors in the circuit using the 'Perform electrical rule check' icon on the toolbar before proceeding further.

c) Assigning footprints

Once it is confirmed that there are no errors in the schematic, the next step in designing a printed circuit board is to assign footprints to each and every component in the circuit. For this purpose, the 'Assign PCB footprints to

schematic symbols' icon should be used. The required footprint should be selected from the list of footprints. If the required footprint is not available, one can add new footprints manually by accessing the 'footprint editor' and adding the new footprint. In this project, the footprint was assigned according to the availability and function of the components used.

d) Generate netlist

Generating the netlist is one of the most important steps in PCB designing. A netlist is a text file that contains all the necessary information about each component within the circuit, including footprint information and details regarding the pin connections. The netlist needs to be added into the PCB editor in order to generate the PCB layout. The 'Generate Netlist' icon in the toolbar enables us to perform this step.

e) PCB layout

Once the netlist is available, one can move to the main part of PCB design, i.e. creating the PCB layout. By making use of the 'pcb layout editor' or 'run Pcbnew' icon in the toolbar, one will be redirected to a new page Pcbnew, in which one needs to import the generated netlist. All the components will now be visible on the page along with lines showing the connections between them. The components can be rearranged in an optimal way according to the required dimensions of the board and the required layers can be applied. The connections between all the components need to be done manually by placing tracks of the necessary width. Once all the connections are made within Pcbnew, one needs to make sure that there are no errors by using 'Design rule checks' icon and with that, the design of the board is complete. The resulting layout of the printed circuit board can be further viewed in 3-Dimension using the '3-D viewer' icon in the toolbar.

f) Create Gerber files

Once the PCB is complete, one can generate Gerber files for each layer using the ‘Gerber’ icon in the toolbar of Pcbnew. The Gerber files created need to be send to a PCB manufacturer, who uses the files to manufacture the board.

g) Generate Bill of Materials

The final step in the design for printed circuit board is the generation of the bill of materials which can be done using ‘generate the bill of materials’ icon in the toolbar.

5.3 Circuit Diagram

The first step in the design of a printed circuit board is the implementation of the circuit diagram or the schematic as explained in the previous section. The schematic for the version 3 board is elaborated in this section. The schematic of the version 3 board is mainly consisting of three sheets, namely the diodes sheet, amplifier sheet and the filter_decoupler sheet.

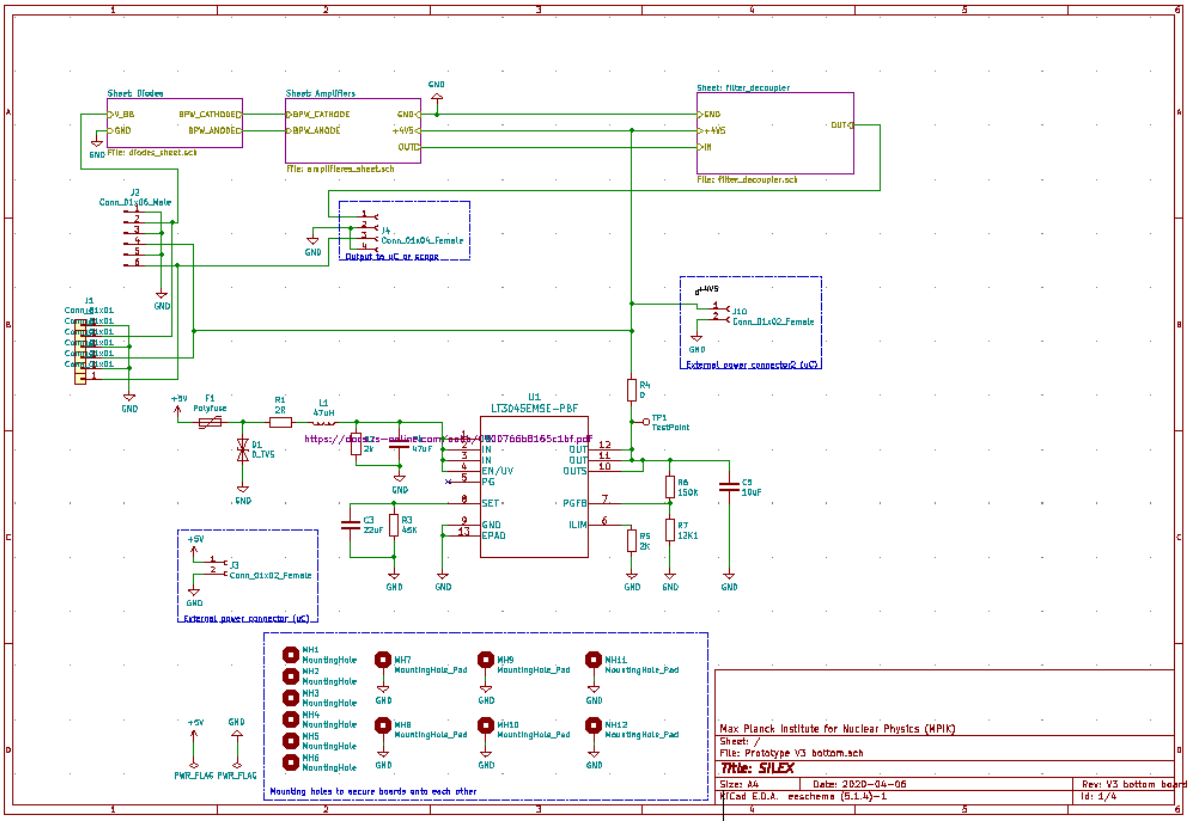

Fig 33. Schematic for bottom board

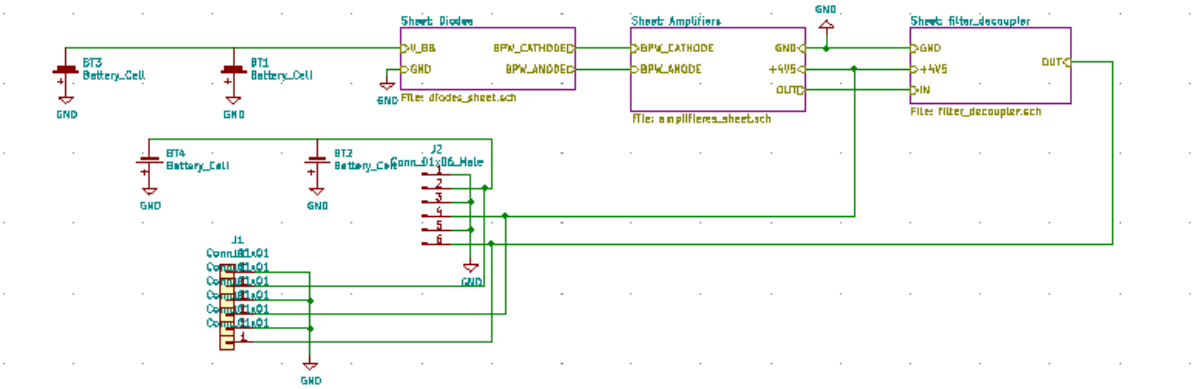

Fig 34. Schematic for top board

Note: the enlarged images of all the schematics are included in the appendix

The schematic of the bottom board, consists of four connectors and an additional circuit which is the voltage regulator circuit other than the three main sheets. The three sheets shown in the circuit will be elaborated later on. The voltage regulator used in the circuit is an LT3045 chip. The circuit for the voltage regulator was identified from the data sheet of LT3045 and the modifications added were according to the performance requirements as recommended in the data sheet. The main modifications to the basic voltage regulator circuit in the data sheet are explained below. The polyfuse and the transient voltage suppression diode (D1) is added at the input in order to provide over-voltage protection. If there are voltage fluctuations and excessive voltage is supplied, then the diode shorts itself such that the excessive voltage is grounded, thereby preventing any of the following components from being damaged. Taking a closer look into the voltage regulator circuit, it can be seen that a 4.7uF capacitor is used in the input pins of LT3045 (pin 1,2,3) along with R1, R2 and L1. Together, they function as a filter circuit [16] [17] which removes noise components in the voltage supply. The 4.7 uF capacitor also functions as a bypass capacitor as the battery's output impedance increases with frequency which might result in a voltage drop of the input supply. The SET pin (pin 8) is the regulation set-point

for the LT3045. The LT3045's output voltage is determined by VSET = ISET * RSET. Adding a capacitance of about 22uF improves output noise, power supply rejection ratio (PSRR) and transient response. Pin 10, 11 and 12 are responsible for supplying load to the output and require an output capacitance of at least 10 uF for stability.

The connector J10 in the circuit was placed as an alternative to supply input voltage directly from the USB to the board. The connector J4 in the Figure 33 is the output connector pins (output of both the top board and the bottom board). In Figure 34, there are 4 additional batteries. The batteries BT1, BT2 are 9V batteries and BT3, BT4 are 12V batteries which are used to supply the bias voltage to the diodes. As per the design only either the 9V or 12V batteries can be mounted at the same time. The connectors J1-J7 and J2 in Figure 33 and 34 are used to supply (a) the 4.5V power supply to the top board, (b) bias voltage from the 12V/9V batteries to bottom board and (c) the top board output to connector J4 in the bottom board. The J2 connectors are female connectors which require extra wires to connect both boards whereas J1-J7 are spring connectors that do not require additional wires.

5.3.1 Diodes sheet

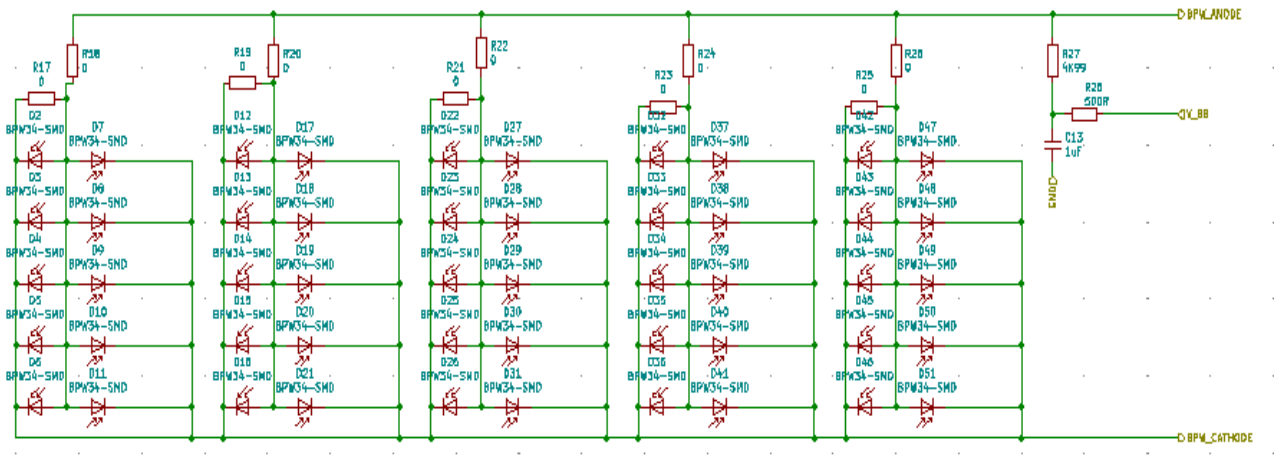

Fig 35. Schematic of diode sheet of bottom board

Figure 35 shows the schematic of diode sheets of the bottom board. It includes 50 PIN-diodes connected in parallel which are used to detect the incoming cosmic ray muons. As the number of diodes increases, the area for muon detection increases. Hence, the circuit accommodates a maximum of 50 diodes which equates to a detection area of approximately 4 cm^2. The resistors R17 to R26 are placed as switches, which can be removed in order to test the board with a lower number of diodes. The schematic of the diodes sheet for the top board is the same as that of the bottom board.

An important parameter to be considered in the design is the dark current. The dark current depicts the charge generated in the PIN-diode detector when no outside radiation is reaching the diodes. The capacitor C7 in Figure 36 blocks the dark current from entering the amplifier circuit and is thus, only prevalent in the diode sheet. In order to calculate the dark current, the voltage across the resistor R27 was measured using a digital volt meter (DVM) and was obtained as,

V_{R27} = 0.04 mV

R27 = 4.99 kOhm

The dark current, I_{dark} is given by,

$$I_{dark} = \frac{V_{R27}}{R27} = \frac{0.04*10^{-3}}{4{\cdot}99*10^{3}} = 8.016 \text{ nA}$$

The dark current that is obtained as a result of 50 PIN diodes and is calculated to be 8.016 nA. Thus, the dark current generated by a single diode is approximately equal to 0.2 nA.

5.3.2 Amplifier sheet

The circuit diagram of the amplifiers used in the version 3 board is the same as that used in version 2 board and is depicted in Figure 36. It can be seen that it consists of two stages of amplifier. The only extra addition in this circuit are test

points in the output of first amplifier stage and the second amplifier stage. A capacitor was also added in the feedback loop of the second amplifier stage. This capacitor was added just in case one needed to test different time constants in the second stage amplifier and is currently not used.

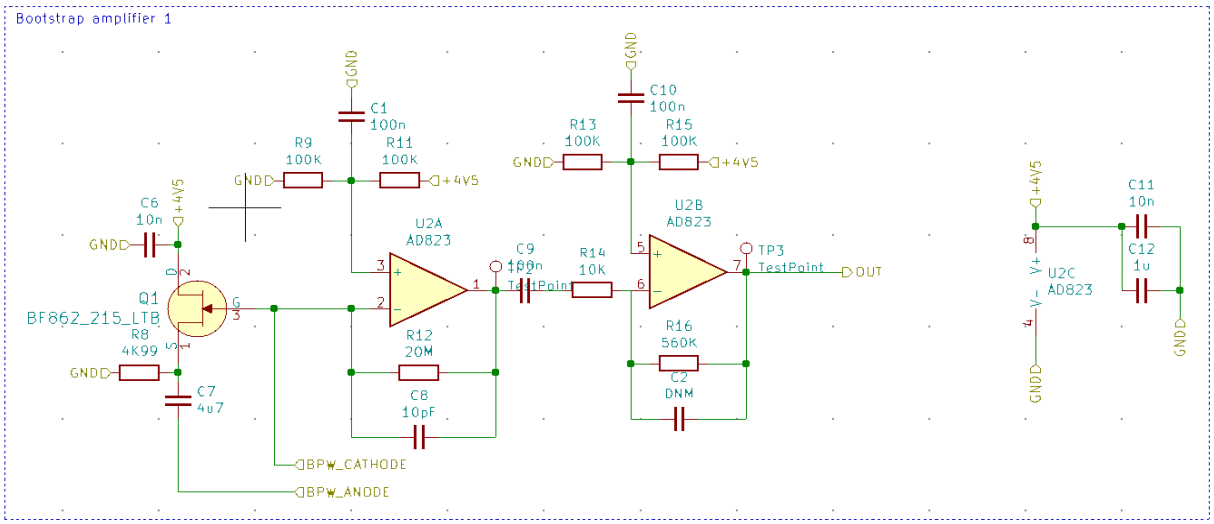

Fig 36. Schematic of Amplifiers sheet of bottom board

It can be seen that the amplifier used for the Silex detector consists of two amplifier stages. The outputs from the anode and cathode of the PIN-diodes are fed into a junction field effective transistor (JFET). Each PIN-diode has a capacitance of about 15pF and the 50 diodes together generates a capacitance equal to 15pF * 50 = 750pF, which has a significant effect on the noise performance of the circuit. The JFET is bootstrapped [13] as shown in the figure in order to improve the noise generated as a result of the large capacitance in the diodes. The signal coming from the JFET undergoes two stages of amplification giving an easily measurable voltage output. Both amplifying stages use inverting op-amps. The circuit diagram and the working of the amplifiers sheet is also the same for the top board and is included in the appendix.

5.3.3 Filter_decoupler sheet

The final sheet in the schematics for the top and bottom board of version 3 board is the filter_decoupler sheet. It consists of the filter circuit and the impedance de-coupler circuit which was implemented and elaborated on in Section 4.3.2 and 4.3.3.

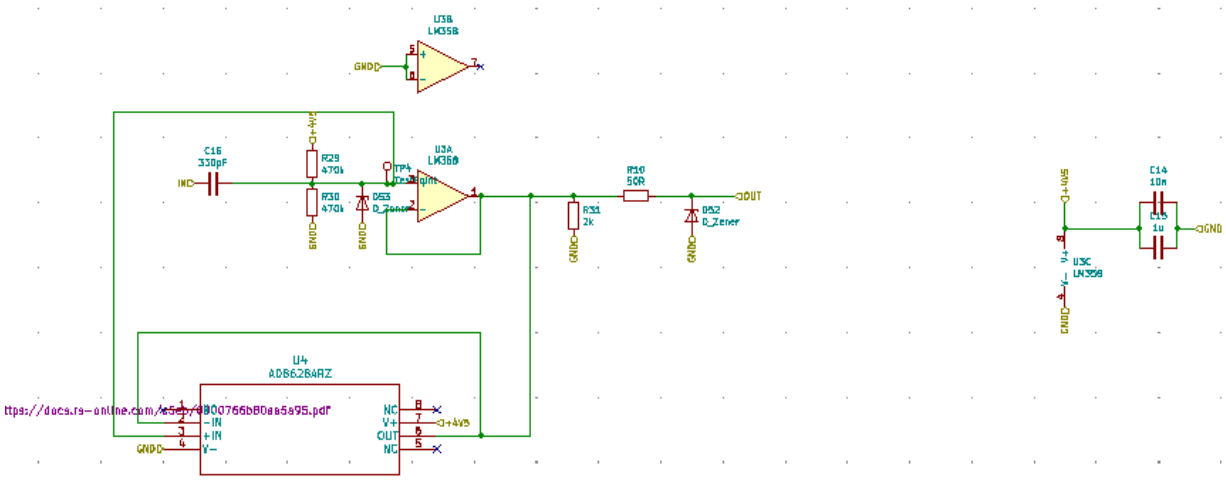

Fig 37. Schematic of filter_decoupler sheet of bottom board

The filter circuit used is the same high-impedance high-pass filter which was tested as a modification to the version 2 board. It is responsible for the removal of noise in the low-frequency range. The impedance decoupling circuit is also the same with the only difference being the addition of an AD8628ARZ. The AD8628ARZ is used as an alternative for the LM358 that was previously used. The same issue, which was explained in section 4.3.4, is valid in this case as well. The voltage range of the LM358 is limited to 0 to 3V. If the signal goes above 3V, then the output signal will be distorted and when used with the ADC, the resolution decreases. Also, we require only a single op-amp in the impedance de-coupler. Hence, the AD8628ARZ as an alternative op-amp was selected due to its good rail-to-rail voltage and for containing a single op-amp within the package as is required by the circuit. The main change in the circuit from that used in version 2 board is the addition of two Zener diodes in the output of filter

and the decoupler stages. This is to provide protection to the following components against high voltages that might appear in the circuit. Since the output of the filter_decoupler circuit will be supplied to the ADC, the Zener diode prevents any high voltage outputs from reaching the ADC. In case a high output voltage appears, the Zener diode acts as a short and prevents the ADC from being damaged. The schematic for the filter_decoupler sheet for the top board is again the same.

5.4 Assigning footprints

Once the circuit design was implemented, footprints were assigned to each and every component in the circuit. Most of the component footprints were selected depending on the availability of the components within the lab. The preferred footprint size for all the capacitors and resistors was 0603. This indicates that the component has dimensions (0.06 inches * 0.03 inches). Few elements were available in the lab only with footprint size 0805. The footprint for the input capacitance (C3) in the voltage regulator was set to 1205 as it prevents the circuit from being damaged when there are voltage fluctuations since it can withstand up to 25V from the power supply. The footprint for the components that were not available were added using the footprint editor. Once assigning the footprint was complete, the netlist for the entire circuit was generated in order to proceed further in to laying out the printed circuit board of version 3 board.

5.5 PCB Layout

The main step in designing the version 3 board is the conversion of the schematic into a PCB layout. The netlist generated was imported into PCBnew. All components were first arranged to fit within the dimensions of the top board and the bottom board. The dimension should be 120 mm * 100,3 mm or very

slightly lower than this for the bottom board in order to be placed accurately within the enclosure. Figure 38 shows the PCB layout of the bottom board.

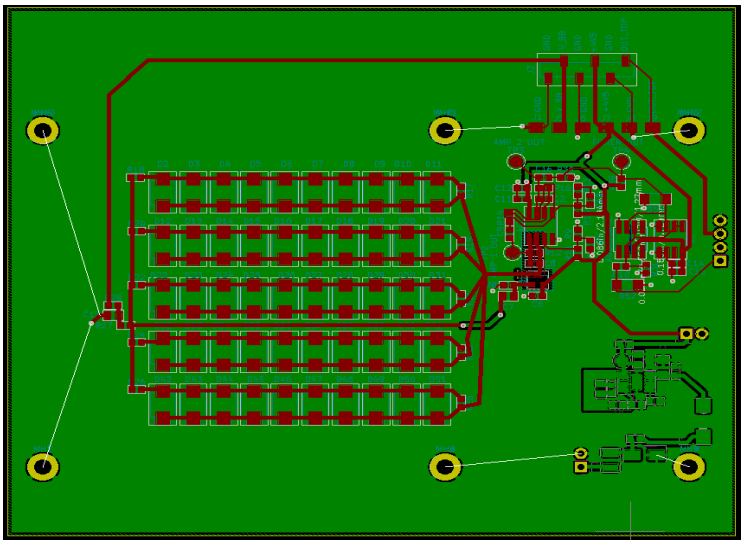

Fig 38. PCB layout of version 3 bottom board

The top board needs to be slightly smaller than the bottom board. The dimensions for the final PCB was 119.38 mm * 99.57mm for the bottom board and 114.30mm * 76.2mm for the top board and edge cuts were placed at these borders. The PCB layout of the top board is shown in Figure 39.

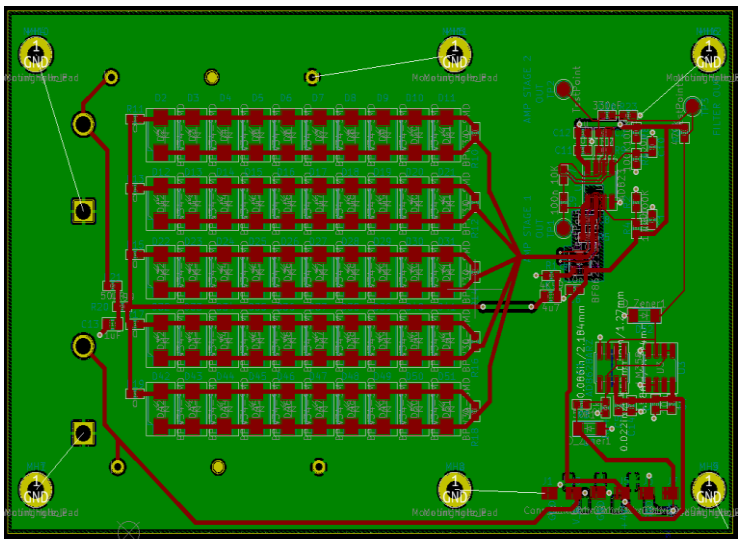

Fig 39. PCB layout of version 3 top board

The thickness of the new board is fixed to 0.8 mm in order to match with the trace thickness around the diodes, such that we get 50 Ohm trace impedance. The main constraint to be considered while placing the components on the top

board and the bottom board was that the diodes on the top board and the bottom board should be placed exactly opposite to each other. These criteria needed to be fulfilled in order to check for coincidences. KiCAD has an option to control the placement of the components using Python. To ensure that the diodes were exactly facing each other, they were placed using a placement script. The entire script was written in Python and then imported into KiCAD. The exact position and the number of diodes in each row were as given in the placement script.

The placement script has functions to place the components in vertical rows, horizontal row and to set its orientation. There is also a function to get the list of diodes (D1 to D50). In the design of the version 3 board, it was decided to arrange 10 diodes in each rows. Therefore, a total of 5 rows with 10 diodes in each row was to be placed. The labels of each of the 10 diodes were loaded into a variable, and each of the variables were given into the function to place components in horizontal rows thereby arranging the diodes within the variable in a horizontal row. The orientation was also set for each of the variables. The same parameters were used in placing the diodes in the top board as well making sure that the diodes in the top board and the bottom board face each other exactly.

Another point to be considered was the placement of the JFET. The JFET should be placed such that it is almost equi-distant from the diode outputs. The connections to the JFET were thus created in a star-like way. It was also essential to place L1 as far away from anything on the output side of the linear regulator as possible, since the traces are prone to inductive coupling via the magnetic field that L1 produces.

Another major change was the addition of a cut out region around the amplifier inputs. This was done in order to ensure minimal loss of charge to capacitive coupling to the bottom side of the board.

The size of the track to make the connections were set to 0.25mm. The connections between the diodes and the connections for the voltages were assigned a track width of 0.7 mm which corresponds to an impedance of about 50 Ohm for a 0.8 mm thick board.

Texts were added on to the backside of the PCB which consist of general information about the board and how to use it. Once the tracks were connected completely and the board was complete, the printed circuit board can be viewed in 2-D and 3-D and is shown in 2-D in Figure 38 and 39.

The Gerber files were then created and the boards were manufactured using the files. The bill of the materials were also generated and is attached in the appendix.

Figures 40 and 41 shows the top board and the bottom board of the version 3 design that were manufactured. The boards were soldered with all the coponents and the final boards are represented in the figure.

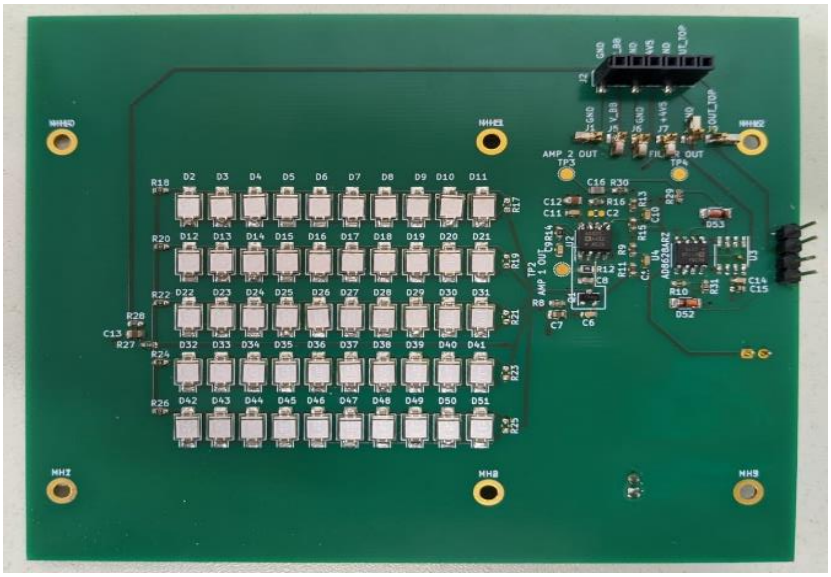

Fig 40. Final PCB for Bottom board

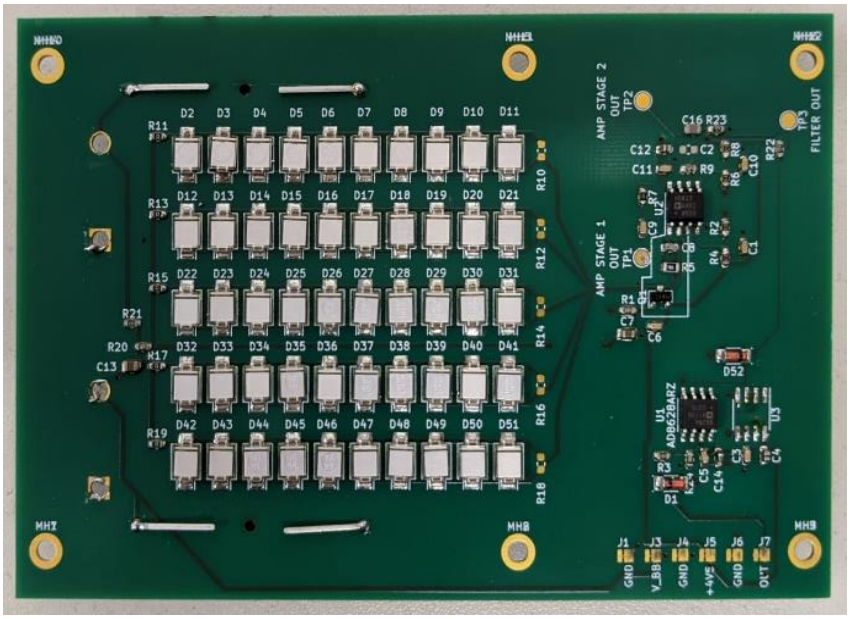

Fig 41. Final PCB for Top board

5.6 Board Set-Up

The board set up for coincidence measurement is as shown below. The 12V batteries are connnected to the top board and the USB power supply is applied to the bottom board. The spring connectors between the top board and the bottom board facilitate the availablity of the 12V bias voltage and power supply to be accessed by both boards. The output of the top board is also given to the bottom boards J4 connector pin in order to make both signal ouputs available on one side of the stacked boards. When stacked together, the boards are kept in place using screws. The boards are then placed inside an enclosure which is grounded. The entire board set up utilizes as few wires as possbile, which makes the entire set up much more organized than the version 2 board set up. The enclosure in which the boards are placed is then closed to avoid light from reaching the PIN-diodes. The set up is placed on top of the scintillator boxes of the CosMO detector right above the scintillator material in order to ensure the detection of coincidences.

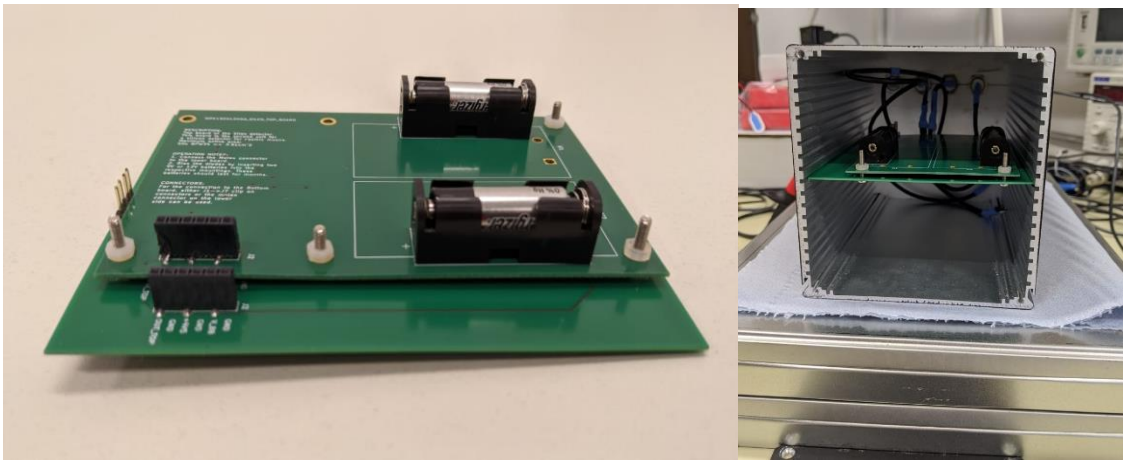

Fig 42. Board Set up (a) top board and bottom board arranged to do the coincidence measurement (b) bottom board and top board placed in the enclosure

5.7 Outputs and Observations

The output pins of the top board, bottom board and the Cosmo detector are connected to the oscilloscope to obtain the output signals. The output signals were tested with different combinations of resistors and capacitors in the feedback loop of the first amplifier stages. The combinations that were tested are (a) 1 MOhm with 6.8 pF, 10 pF, 15 pF (b) 10 MOhm with 6.8 pF, 10 pF, 15 pF and (c) 20 MOhm with 6.8 pF, 10 pF and 15 pF in the feedback loop. A thourough analysis was conducted by my colleague, Priyanka Kesavadas, using the data obtained from the coincidence measurements. In conclusion of this analysis the 20M resistor and 10pF capacitor combination in the feedback loop was found to provide the best performance.

A muon passing through 100µ of Silicon will create a measurable charge of approximately 11000 electrons, which is equal to 1.76 * 10^{-15} C. (same as in Section 4.5). The voltage,

$$V = \frac{Q}{C} = \frac{1{\cdot}76{*}10^{-15}}{10{*}10^{-12}} = 0.17\,mV$$

When this signal passes through the second amplifier stage which has a gain of 56, the total voltage

V= 0.17 * 56 = 9.52 mV

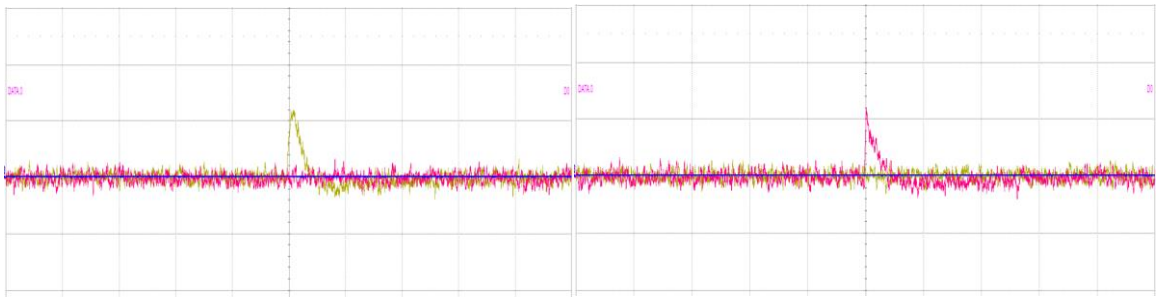

(a) (b)

Fig 43. Output signals for version 3 board with 20Mohm resistance and 10pF capacitance in the feedback loop of amplifier with signal on (a) Bottom board (b) Top board *[X-axis = 10us/div and Y-axis = 50mV/div]*

Figure 43 shows the output signals obtained using version 3 board with 20 MOhm resitance and 10pF capacitance in the feedback loop. The yellow graph represents the output signal for bottom board and the red graph shows the output signal for the top board. The Figure 43 (a) is obtained when the trigger is applied to the bottom board and Figure 43 (b) is obtained when the trigger is applied to the top board.

It can be observed from the output signal that it has good signal quality and that the circuit works fine. The output signal is about 60 mV and is clearly distinguishable from the noise. The output signal varies from the expected 9.52mV due to fluctuations in the energy loss. The trigger applied causes large signals to be selected and there are also signals not associated to muons which are larger than genuine muon signals. The noise levels are also much lower than in the previous board design.

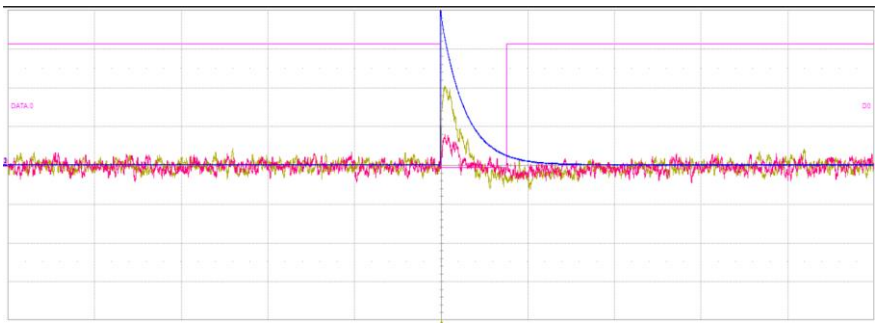

Fig 44. Graph showing coincidence between top board (red), bottom board (yellow) and Cosmo detector (pink and blue) with trigger on bottom board *[X-axis = 100us/div and Y-axis = 50mV/div]*

Figure 44 shows a coincidence between the top board, the bottom board and the CosMO detector when a trigger is applied to the bottom board. An output signal is generated when a particle passes through the detector. A coincidence means that a particle likely passed through all the three detectors, i.e., the particle passed through the top board, bottom board and the Cosmo detector as well.

The noise level in the output can be analysed by taking the spectrum of the output signal.

Figure 45 shows the FFT of the output signals of version 3 board. It can be observed that there are no noise components in frequency range of 100 KHz and 1 KHz. A noise of about 20dB is visible in lower frequency levels in Figure 45 (a) but is much lower than the previous version 2 board.

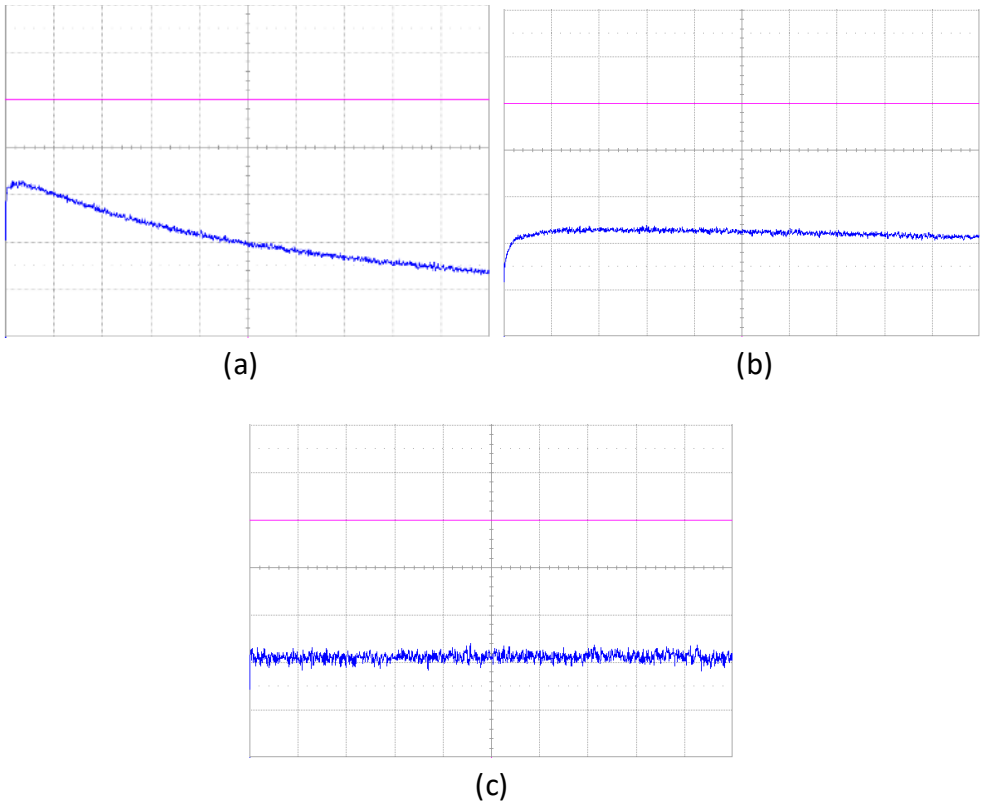

(a) (b)

(c)

Fig 45. FFT for output signal of Silex version 3 board having Y-axis = 10dB/div and X-axis having a span of (a) 1MHz (b) 100KHz (c) 1 KHz

The background noise in the spectrum is much lower when compared to version 2 board spectrum. The peaks or harmonics that appeared in Silex version 2

board which was observed as a result of ambient light entering the enclosure is also not present in the lower frequency ranges. The design thus proves to be much better than the previous board versions.

Rise Time:

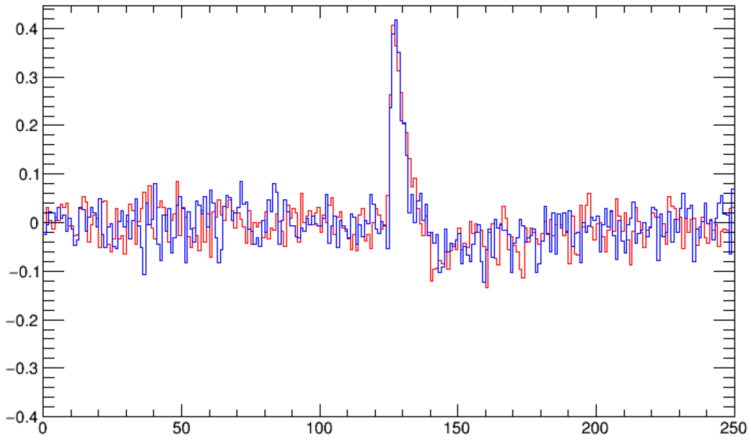

Fig 46. Averaged and normalised signal for version 3 Board [22]

Figure 46 shows the averaged and normalised (20M resistance and 10pF capacitance in the feedback loop) signal obtained from the coincidence measurement. The x-axis consists of 250 samples, which is equal to a total span of 1ms.

The time duration for one sample is

T = 1ms/250

= 4µs

For the signal to rise from 10% to 90%, it takes approximately 2 samples.

The rise time is obtained as

$T_{rise} = T_{10\%}$ to $T_{90\%}$

$T_{rise} = 2 * 4\mu s$

$= 8\mu s$

The rise time of version 3 board (8µs) is lesser than that of version 2 board (14µs) which indicates that the signal rises faster in version 3 board.

CHAPTER 6

CONCLUSION

A cosmic ray muon detector, named Silex is developed in order to make it accessible to general public at low cost. The shortcomings of the version 2 board, from which this Master Thesis began were resolved. In order to improve the signal quality, a high-pass filter circuit was implemented along with an impedance decoupling circuit for impedance matching. The high-pass filter removes the low-frequency noise components and changing the op-amp in both amplifier stages further stabilizes the performance of the board. All changes and modifications to the version 2 board were incorporated into the design of the new Silex version 3 board. The version 3 board produces output signals with very good signal quality and significantly less noise. The various changes incorporated into the design further improved the signal quality. The output signal is clearly distinguishable from noise. It can thus be concluded that the new version 3 board for the Silex detector was a success. The next step that is to be taken in the development of the Silex detector is the addition of a microcontroller unit to make it accessible to the general public as a product. The detector can then be introduced to schools and offices at a price tag of about 100 Euro, which makes it feasible for general public.

REFERENCES

[1] Detection of the Angular Distribution of cosmic ray muons and Development of a low-cost Silicon Detector, Hendrik Borras Link : https://pure.mpg.de/pubman/faces/ViewItemOverviewPage.jsp?itemId=item_2573792_ [June,2020]

[2] https://commons.vccs.edu/cgi/viewcontent.cgi?article=1087&context=exigence [June,2020]

[3] https://home.fnal.gov/~group/WORK/muonDetection.pdf [June,2020]

[4] https://www.phys.ufl.edu/courses/phy4803L/group_I/muon/muon.pdf [July,2020]

[5] Paola La Rocca, Domenico Lo Presti and Francesco Riggi (August 22nd 2018). Cosmic Ray Muons as Penetrating Probes to Explore the World around Us, Cosmic Rays, Zbigniew Szadkowski, IntechOpen, DOI: 10.5772/intechopen.75426. Available from: https://www.intechopen.com/books/cosmic-rays/cosmic-ray-muons-as-penetrating-probes-to-explore-the-world-around-us [June,2020]

[6] https://www.electrical4u.com/p-i-n-photodiode-avalanche-photo-diode/ [June,2020]

[7] http://cosmicpi.org/ [June,2020]

[8] https://www.desy.de/school/school_lab/zeuthen_site/cosmic_particles/experiments/cosmo_experiment/index_eng.html [June,2020]

[9] https://pubmed.ncbi.nlm.nih.gov/31581431/ [June,2020]

[10] R. Franke, M. Holler, B. Kaminsky, T. Karc, H. Prokoph, A. Schonwald¨, C. Schwerdt, A. Stossl¨ , M. Walter, ”CosMO – A Cosmic Muon Observer Experiment for Students “, 33rd International Cosmic ray conference, Rio De Janeiro, 2013, Link- https://arxiv.org/pdf/1309.3391.pdf [June,2020]

[11] https://www.ti.com/lit/an/slyt213/slyt213.pdf?ts=1596153466160&ref_url=https%253A%252F%252Fwww.google.com%252F

[12] https://docs.kicad-pcb.org/5.1/en/getting_started_in_kicad/getting_started_in_kicad.html [July,2020]

[13] https://www.analog.com/media/en/technical-documentation/data-sheets/6244fb.pdf [July,2020]

[14] https://www.analogictips.com/improving-transimpedance-amplifiers-bootstrap/ [August,2020]

[15] https://www.ti.com/lit/an/slyt213/slyt213.pdf?ts=1596153466160&ref_url=https%253A%252F%252Fwww.google.com%252F [July,2020]

[16] http://www.bndhep.net/Lab/Filter/Filter.html [July,2020]

[17] http://sim.okawa-denshi.jp/en/RLClowkeisan.htm [July,2020]

[18] https://www.microchip.com/developmenttools/productdetails/atsame54-xpro [July,2020]

[19] https://en.wikipedia.org/wiki/USB_hardware#Power [August,2020]

[20] https://www.webcitation.org/685PPTw8f?url=http://www.usb.org/developers/docs/ [July,2020]

[21] Private communication with Hendrik Borras

[22] Private communication with Priyanka Kesavadas

LIST OF FIGURES

APPENDIX

1. Code for placement of diodes on the board

```
# general settings
add_reload_button = False
module_name = "place"

# generic imports
import pcbnew
from pcbnew import FromMM, wxPoint

# Add the reload button to the menu
if add_reload_button:
    import sys
    import wx
    import wx.aui

    # get the path of this script. Will need it to load the png later.
    import inspect
    import os
    filename = inspect.getframeinfo(inspect.currentframe()).filename
    path = os.path.dirname(os.path.abspath(filename))
    print("running {} from {}".format(filename, path))

    def findPcbnewWindow():
        windows = wx.GetTopLevelWindows()
        pcbnew = [w for w in windows if w.GetTitle()[0:6] == "Pcbnew"]
        if len(pcbnew) != 1:
            raise Exception("Cannot find pcbnew window from title matching!")
        return pcbnew[0]

    pcbwin = findPcbnewWindow()
    top_tb = pcbwin.FindWindowById(pcbnew.ID_H_TOOLBAR)
    def MyButtonsCallback(event):
        # Removes the old button and then reloads the module
        # In the hope that the dev changed something
```

```
        top_tb.DeleteTool(itemid)
        top_tb.Realize()
        reload(sys.modules[module_name])

    bm = wx.Bitmap(path + '/icon.png', wx.BITMAP_TYPE_PNG)
    itemid = wx.NewId()
    top_tb.AddTool(itemid, module_name+" module reloader", bm, "Reloads
the placement script", wx.ITEM_NORMAL)
    top_tb.Bind(wx.EVT_TOOL, MyButtonsCallback, id=itemid)
    top_tb.Realize()

# places components in a vertical row
# all measurements are in mm
# The components must be given as a list of strings, e.g. ["D4", "R2", "C12"]
# They are then placed in a vertical row from the point x_start, y_start on
# And at each step y_step
def place_vertical_row(references_list, x_start, y_start, y_step):
    pcb = pcbnew.GetBoard()
    for i in range(len(references_list)):
        # get the part
        part = pcb.FindModuleByReference(references_list[i])
        # set the parts position
        part.SetPosition(wxPoint(FromMM(x_start), FromMM(y_start + y_step*i)))

def place_horizontal_row(references_list, x_start, y_start, x_step):
    pcb = pcbnew.GetBoard()
    for i in range(len(references_list)):
        # get the part
        part = pcb.FindModuleByReference(references_list[i])
        # set the parts position
        part.SetPosition(wxPoint(FromMM(x_start + x_step * i),
FromMM(y_start)))

    # apply the changes in the editor
    #pcbnew.Refresh()
# Sets the orientation in degrees for a list of components
def set_orientation(references_list, orientation_degrees):
```

```
    pcb = pcbnew.GetBoard()
    for i in range(len(references_list)):
        # get the part
        part = pcb.FindModuleByReference(references_list[i])
        # set the parts position
        part.SetOrientationDegrees(orientation_degrees)

    # apply the changes in the editor
    #pcbnew.Refresh()
# Gets the reference labels for multiple diodes,
# This works in the same way as range(start, stop, step)
# gets multiple numbers. Just with the Diode labels.
def get_diode_labels(start, stop, step=1):
        diodes = list(range(start, stop, step))
        diodes = map(lambda x: "D"+str(x), diodes)
        return diodes

list_of_diodes1 = get_diode_labels(2,12)
list_of_diodes2 = get_diode_labels(12,22)
list_of_diodes3 = get_diode_labels(22,32)
list_of_diodes4 = get_diode_labels(32,42)
list_of_diodes5 = get_diode_labels(42,52)

place_horizontal_row(list_of_diodes1, 43.18, 42.23, 5)
place_horizontal_row(list_of_diodes2, 43.18, 52.23, 5)
place_horizontal_row(list_of_diodes3, 43.18, 62.23, 5)
place_horizontal_row(list_of_diodes4, 43.18, 72.23, 5)
place_horizontal_row(list_of_diodes5, 43.18, 82.23, 5)

#diodes_to_reorient = get_diode_labels(2, 7)
set_orientation(list_of_diodes1, 90)
set_orientation(list_of_diodes2, 90)
set_orientation(list_of_diodes3, 90)
set_orientation(list_of_diodes4, 90)
set_orientation(list_of_diodes5, 90)
# show changes in the editor
pcbnew.Refresh()
```

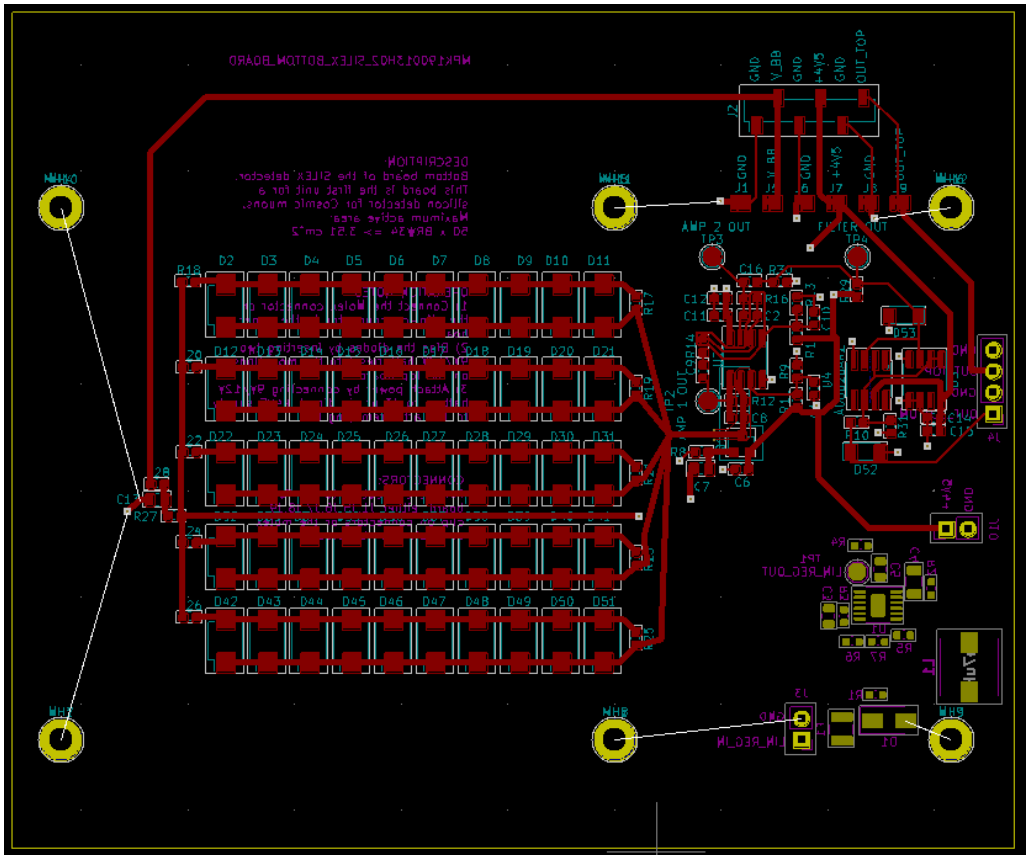

Fig : PCB Layout for bottom board

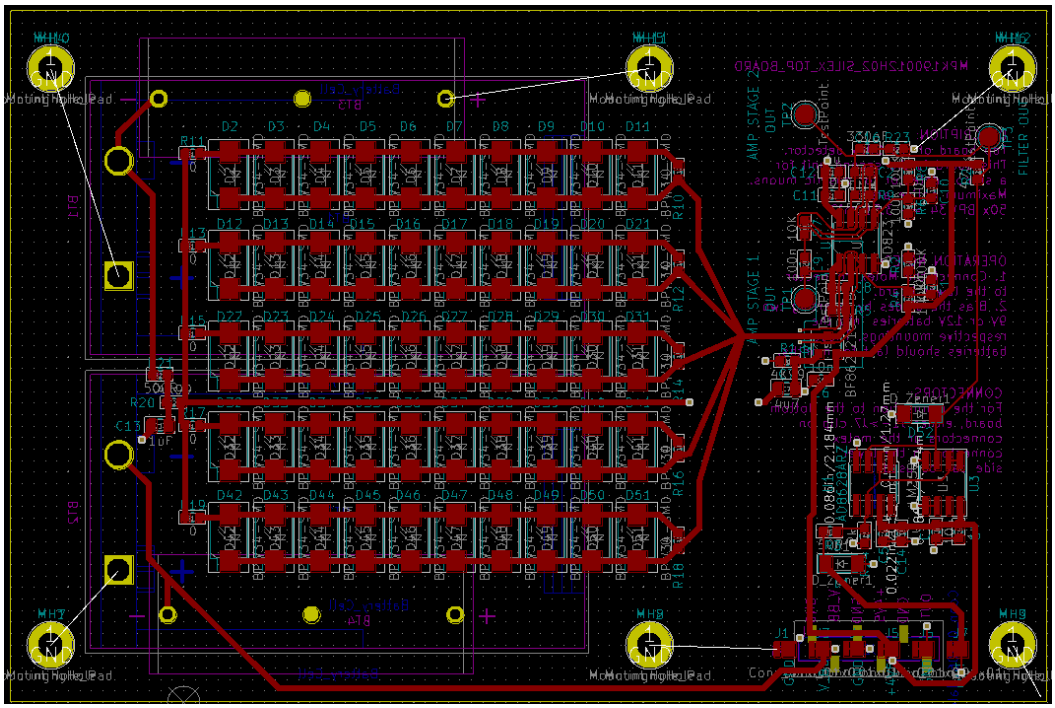

Fig : PCB Layout for top Board

KICAD FLOW_CHART

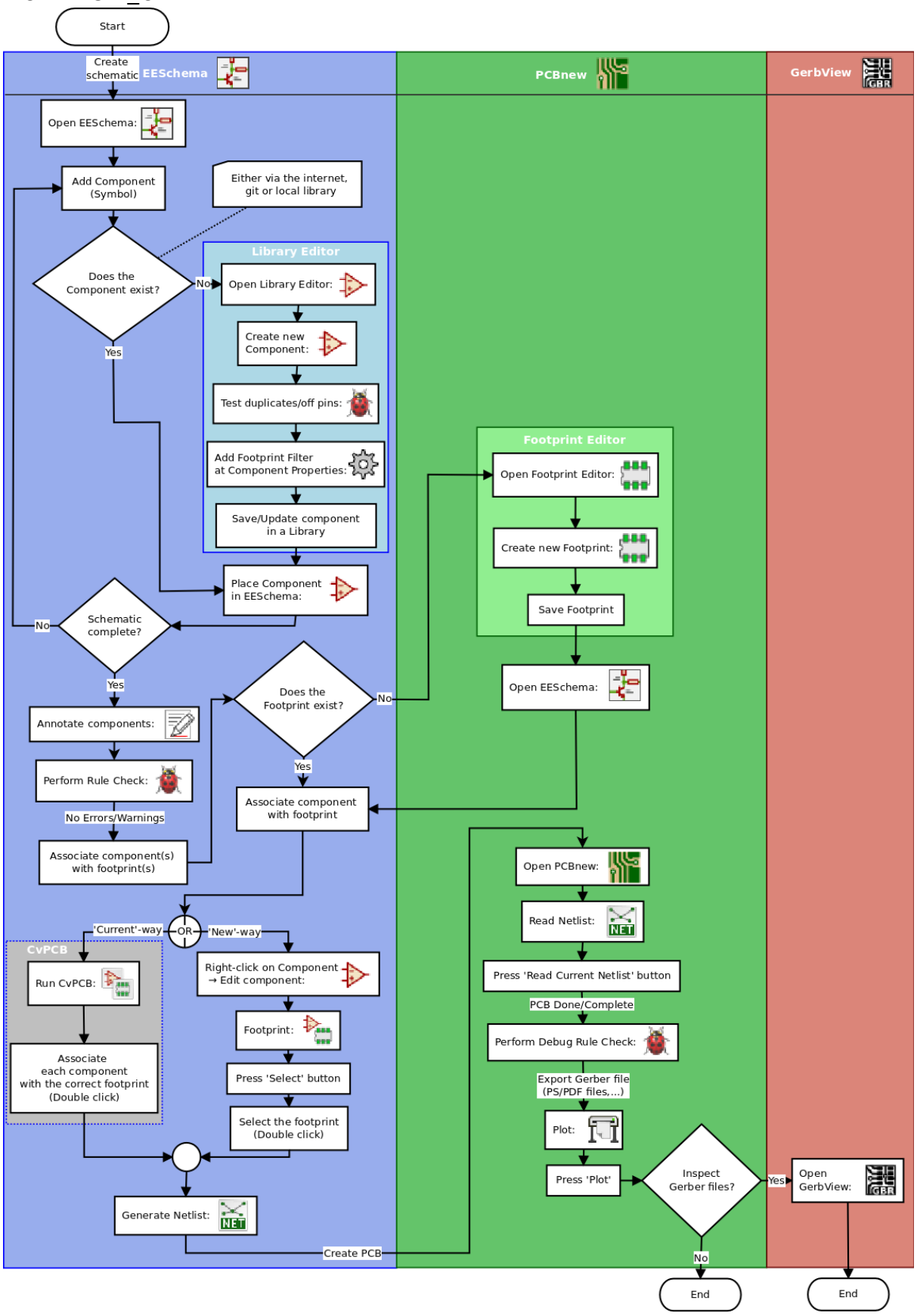

Fig : Flow chart for PCB designing using KiCAD [8]